PHYSICAL REVIEW B **79**, 184507 (2009)

# Critical charge dynamics of superconducting $La_{2-x}Sr_xCuO_4$ thin films probed by complex microwave spectroscopy: Anomalous changes of the universality class by hole doping

T. Ohashi
*Department of Basic Science, The University of Tokyo, 3-8-1 Komaba, Meguro-ku, Tokyo 153-8902, Japan*

H. Kitano*
*Department of Physics and Mathematics, Aoyama Gakuin University, 5-10-1 Fuchinobe, Sagamihara, Kanagawa 229-8558, Japan*

I. Tsukada
*Central Research Institute of Electric Power Industry, 2-11-1 Iwadokita, Komae, Tokyo 201-8511, Japan*

A. Maeda
*Department of Basic Science, The University of Tokyo, 3-8-1 Komaba, Meguro-ku, Tokyo 153-8902, Japan*
(Received 22 October 2007; revised manuscript received 14 April 2009; published 7 May 2009)

We study the critical charge dynamics of the superconducting to the normal-state transition for $La_{2-x}Sr_xCuO_4$ (LSCO) thin films with a wide range of the Sr concentration by measuring the frequency-dependent excess parts of the complex microwave conductivity, which is induced by the superconducting fluctuations. We present a dynamic scaling analysis of the complex fluctuation conductivity, which includes the information on the universality class and the dimensionality of the critical charge dynamics as a function of the Sr concentration, the film thickness, and the magnetic field. In our previous study [H. Kitano *et al.*, Phys. Rev. B **73**, 092504 (2006)], the two-dimensional (2D)-*XY* critical dynamics for underdoped LSCO and the three-dimensional (3D)-*XY* critical dynamics for optimally doped LSCO were reported. In this study, we observed a two-dimensional unknown critical charge dynamics for overdoped thin films from $x=0.17$ to 0.20, which is clearly distinguished from the 2D-*XY* critical dynamics. Through the systematic measurements by changing the film thickness or by applying small magnetic field, it was confirmed that this unusual behavior, which is referred as 2D-"U" below, was not induced by the finite-size effect but was intrinsic to the overdoped LSCO. Thus, it was found that the critical behavior in the phase diagram of LSCO is classified into the following three types: (i) 2D-*XY* for underdoped region, (ii) 3D-*XY* for optimally doped region, and (iii) 2D-"U" for overdoped region. In other words, the dimensionality in the critical charge dynamics is changed twice with hole doping. We discuss possible origins of such anomalous dimensional crossovers with hole doping, including an interpretation based on the possible existence of a hidden quantum critical point near the optimally doped region.

DOI: 10.1103/PhysRevB.79.184507 PACS number(s): 74.25.Nf, 74.40.+k, 74.72.Dn, 74.78.Bz

## I. INTRODUCTION

One of the most striking features in the cuprate superconductors is the strong doping dependence of the critical temperature, $T_c$. It is well known that a plot of $T_c$ versus the carrier doping forms a bell-shaped phase diagram. In spite of a large number of experimental and theoretical studies on this issue, the physical origin of the phase diagram including the pseudogap phenomena above $T_c$ in the underdoped region is still debated.

When we focus on a role of quantum criticality (QC) in the phase diagram of high-$T_c$ cuprates, most of theoretically proposed phase diagrams can be classified into the following two groups. In the first group, two quantum critical points (QCPs) are recognized at both end points of the superconducting transition line. However, the bell-shaped superconducting dome or anomalous properties in the pseudogap regime is explained by a different concept from the QC, for instance, the gauge-field fluctuations in the $t-J$ model[1,2] or the classical phase fluctuations of superconducting orders, which are assumed to survive even in the pseudogap regime.[3]

On the other hand, in the second group, in addition to the two well-established QCPs in the first group, another QCP is assumed to exist (or to be hidden) inside the superconducting dome. In other words, the existence of a hidden order is assumed, which may compete or cooperate with the superconducting order. In this viewpoint, superconductivity and the anomalous behavior in the pseudogap regime are related to the hidden order and its large quantum fluctuation around the hidden QCP. Various candidates for this hidden order have been proposed; for instance, a magnetic Néel order,[4,5] an incommensurate charge-density wave,[6] a time-reversal-violating state,[7] a *d*-density wave,[8] and a charge/spin stripe order.[9,10] Possible candidates for such an unknown order have also been investigated by a more general consideration using a group-theoretic classification for competing orders.[11] Several experiments have suggested a possibility that there is the hidden QCP in the vicinity of the optimally doped concentration.[12–17] However, the interpretation of such experimental results is still controversial and the relationship with a mechanism of superconductivity also remains unresolved.

These two groups contrast strikingly with each other in term of the possibility of a hidden quantum phase transition (QPT). If a typical frequency scale of such a QPT was sufficiently larger than a thermal energy, it is difficult to disen-

 

tangle quantum and thermal effects.[18] This means that the classical critical dynamics can be affected by the quantum-fluctuation effects near the hidden QCP. Therefore, one can know which group is more appropriate for describing the phase diagram of high-$T_c$ cuprates by investigating the superconducting to the normal-state transition with a wide range of carrier doping. Fortunately, the critical fluctuation effects, which reflect the transition nature, can be explored in the high-$T_c$ cuprates because the short coherence length, the small superfluid density, and the quasi-two-dimensionality largely enhance the classical fluctuations of the superconducting order.[19]

In our previous paper,[20] we reported that the critical charge dynamics for underdoped $La_{2-x}Sr_xCuO_4$ (LSCO) from $x=0.07$ to 0.14 was successfully expressed by the two-dimensional (2D)-*XY* universality class, that is, Berezinskii-Kosterlitz-Thouless (BKT) picture.[21] On the other hand, the critical behaviors for almost optimally doped LSCO ($x=0.16$) were found to be expressed by the three-dimensional (3D)-*XY* universality class. This sudden change of the universality class was highly unexpected because the classical critical behavior must be universal, irrespective to the microscopic details such as a carrier concentration.[22]

These anomalous results supported the idea that the systematic measurements of the critical charge dynamics as functions of carrier concentration are quite effective to study the phase diagram of high-$T_c$ cuprates. However, the previous work covered a part of the whole phase diagram. Thus, it is crucially important to complete the investigation including the overdoped region.

Based on these backgrounds, we have investigated the critical charge dynamics of the superconducting to the normal-state transition for high-quality LSCO thin films with a wide range of the Sr concentration. We measured the frequency dependence of the complex microwave conductivity, $\sigma(\omega)=\sigma_1(\omega)-i\sigma_2(\omega)$, which is enhanced by the superconducting fluctuation, under zero and small finite magnetic fields. In this paper, we present results of the critical charge dynamics for optimally doped LSCO ($x=0.15$ and 0.16) and overdoped LSCO (from $x=0.17$ to 0.20). The most important finding was that there is another dimensional crossover from 3D to 2D between $x=0.16$ and $x=0.18$. To clarify the details of this anomalous behavior, the finite-size effects were also investigated by changing the film thickness or by applying small finite magnetic fields. Together with our previous study,[20] we discuss a whole picture of the critical charge dynamics in the phase diagram of LSCO in terms of various proposed models. We consider that the newly found second sudden crossover needs to be explained by assuming the additional hidden QCP near the optimal doping.

This paper is organized as follows. In Sec. II, we summarize the practical merits of a dynamic scaling analysis using the frequency-dependent complex conductivity, comparing to the scaling analyses using other thermodynamic and transport properties. In Sec. III, we briefly describe the preparation of high-quality LSCO thin films and the broadband technique to obtain the frequency-dependent microwave conductivity. Section IV contains all the experimental results on the dependence of the critical charge dynamics on the hole doping, the film thickness, and the magnetic field. In Sec. V, various proposed models are systematically discussed to explain the sets of our data. Finally, we conclude this work in Sec. VI.

## II. DYNAMIC SCALING ANALYSIS OF COMPLEX FLUCTUATION CONDUCTIVITY

The critical behaviors are characterized by the divergence of typical length and time scales in the vicinity of a critical point. In the case of classical phase transition,[22] a correlation length, $\xi$, is often used as the typical length scale. $\xi$ diverges as $\xi=\xi_0|T/T_c-1|^{-\nu}$, where $\xi_0$ is the correlation length at $T=0$ and $\nu$ is a static critical exponent. On the other hand, the divergence of a correlation time, $\tau$, is given by $\tau=\xi^z$. Here, $z$ is a dynamic critical exponent. The divergence of $\xi$ and $\tau$ in quantum phase transition can also be defined in a similar manner, except that a singular point is not a $T_c$ but a QCP at $T=0$.

Fisher, Fisher, and Huse (FFH) (Ref. 19) provided a general formulation of the dynamic scaling hypothesis for the frequency-dependent complex fluctuation conductivity, $\sigma_{\mathrm{fl}}(\omega)$, near the superconducting transition, as follows:

$$\sigma_{\mathrm{fl}}(\omega) \approx \xi^{z+2-d} S(\omega\xi^z). \tag{1}$$

Here, $S(x)$ is a complex universal scaling function and $d$ is a spatial dimension. As was emphasized in our previous paper,[20] the most essential part of our analyses is that we can check the validity of this hypothesis by measuring the frequency dependence of $\sigma_{\mathrm{fl}}(\omega)$. Following a pioneering work by Booth *et al.*,[23] we use both the magnitude, $|\sigma|$, and the phase, $\phi_\sigma(\equiv\tan^{-1}[\sigma_2^{\mathrm{fl}}/\sigma_1^{\mathrm{fl}}])$, of $\sigma_{\mathrm{fl}}(\omega)$ as scaled quantities in the scaling analysis of $\sigma_{\mathrm{fl}}(\omega)$. First of all, the phase part of $\sigma_{\mathrm{fl}}(\omega)$ at different temperatures is scaled by using a normalizing factor, $\omega_0$, along the $\omega$ direction in the plots of $\phi_\sigma$ versus $\omega$. Next, the magnitude part of $\sigma_{\mathrm{fl}}$ as a function of the normalized frequency, $\omega/\omega_0$, is also scaled by using another normalizing factor, $\sigma_0$, along the $|\sigma|$ direction. Note that $\omega_0$ and $\sigma_0$ are independently obtained in our procedure, since we measure data sets of $\sigma_{\mathrm{fl}}(\omega)$ as complex quantities with two independent components.

If the data sets of $\phi_\sigma$ and those of $|\sigma|/\sigma_0$ collapse on to a single universal function of $\omega/\omega_0$, respectively, we find that the dynamic scaling hypothesis is satisfied. Thus, Eq. (1) tells us that the two scaling parameters, $\omega_0$ and $\sigma_0$, can be connected with the diverging length scale, $\xi$, as follows:

$$\omega_0 \propto \xi^{-z} \propto |T/T_c - 1|^{\nu z}, \tag{2}$$

$$\sigma_0 \propto \xi^{z+2-d} \propto |T/T_c - 1|^{-\nu(z+2-d)}. \tag{3}$$

By using these relationships, we can directly determine the two critical exponents, $\nu$ and $z$, and the dimensionality, $d$, through the temperature dependence of $\omega_0$ and $\sigma_0$. On the other hand, if the data sets of $\phi_\sigma$ or those of $|\sigma|/\sigma_0$ do not collapse on to a single curve, we find that the dynamic scaling hypothesis is broken down, so that we cannot extract the information of the universality class from Eqs. (2) and (3). Indeed, we have encountered such a breakdown of the data collapse in $\phi_\sigma$ for the conventional NbN superconducting

thick film, showing a dimensional crossover due to the divergence of $\xi$ beyond the film thickness.[24] We also observed that a broad distribution of $T_c$ caused a breakdown of the dynamic scaling, which will be described in Sec. V

The dynamic scaling procedures described above yield more reliable information than other scaling procedures because of the following reasons. First of all, the scaling procedure of $\phi_\sigma(\omega)$ was performed in a linear scale. This required a stricter criterion in data collapse than ordinary scaling procedures performed in the log-log plots, which easily lead to spurious scaled behaviors. In addition, the dynamic scaling analyses can be performed by using only the experimental data. In other words, we can check whether data obey the scaling hypothesis or not, without any assumption. This is in contrast with other scaling procedures. For example, in the case of the scaling analysis of the *I-V* characteristics,[25] the dimensionality, $d$, has to be assumed first. The value of $z$ is obtained from the limiting behavior of $V(\propto I^{(z+1)/(d-1)})$ at $T_c$. Only after those procedures, data can be scaled in the plots of $(I/T)|T-T_c|^{-\nu(d-1)}$ versus $(V/I)|T-T_c|^{-\nu(2+z-d)}$. The value of $\nu$ is obtained from a successfully scaled behavior of the plots. However, the ambiguity of $T_c$ easily gives rise to large error bars on the obtained results of $z$ and $\nu$, which degrades the reliability of the scaling analysis. In addition, one cannot detect the breakdown of the dynamic scaling hypothesis due to the dimensional crossover in these procedures. Other scaling analyses require the assumption of a particular model in advance to perform the scaling analyses as well, such as, the scaling analysis of the dc magnetization,[26] the specific heat,[27] the thermal expansion,[28] and the ac conductivity at a fixed frequency.[29]

Unfortunately, there was no consensus among the previous results on the superconducting fluctuations of high-$T_c$ cuprates mostly based on the measurements described above. We believe that such controversial results were attributed to the lack of the experimental check on the applicability of the static or dynamic scaling hypothesis. In this sense, only the dynamic scaling analysis of $\sigma_{\rm fl}(\omega)$ is exceptional, since no assumption is needed to check whether the data sets of $\phi_\sigma$ or $|\sigma|$ collapse on to a single curve or not. This is the reason why we adopted this method to investigate the critical charge dynamics near the superconducting transition of high-$T_c$ cuprates as a function of carrier doping.

More precisely speaking, the determination of $\nu$ and $z$ is affected by the ambiguity of $T_c$, even if the dynamic scaling form predicted by FFH is confirmed to be satisfied. However, the determination of the dimensionality, $d$, is free from the ambiguity of $T_c$, since a product of $\omega_0$ and $\sigma_0$ is proportional to $\xi^{2-d}$, as derived from Eqs. (2) and (3). This suggests that $\omega_0\sigma_0$ is independent of $T$ for $d=2$, while it increases with increasing $T$ for $d=3$, since $\nu$ is always positive. In addition, Eq. (1) shows us that the phase angle and the magnitude of $\sigma_{\rm fl}(\omega)$ behave as

$$\phi_\sigma \to \frac{\pi}{2}\frac{z+2-d}{z}, \tag{4}$$

$$\frac{|\sigma|}{\sigma_0} \to \omega^{-(z+2-d)/z}, \tag{5}$$

respectively, as $T$ approaches $T_c$. This limiting behavior is also very useful to discuss the dimensionality. If $d=2$, then $\phi_\sigma \sim \pi/2$ and $|\sigma| \propto 1/\omega$ for $T \to T_c$, independent of $z$. On the other hand, for $d=3$, it is expected that $\phi_\sigma \sim \pi/4$ and $|\sigma| \propto 1/\omega^2$ for $T \to T_c$, since a fully relaxational dynamics with $z \approx 2$ (that is, the so-called model-*A* dynamics in the Hohenberg and Halperin classification[30]) is expected for a charged superfluid.[19] Thus, we can discuss the dimensionality of the superconducting phase transition through the limiting behavior of $\phi_\sigma$ and $\omega_0\sigma_0$ in the vicinity of $T_c$, even if the precise value of $T_c$ is unknown. This is particularly important when we discuss the dimensionality as a function of carrier doping.

TABLE I. Various parameters of LSCO films. $t$ is a thickness, $\rho$ is the resistivity at $T=50$ K, $T_c^R$ is a critical temperature defined by zero resistance, $\Delta T_c$ is the 10%–90% transition width, and $T_c^{\rm sacle}$ was determined from the dynamic scaling analysis, respectively.

| $x$ | $t$ (nm) | $\rho$ (m Ω cm) | $T_c^R$ (K) | $\Delta T_c$ (K) | $T_c^{\rm scale}$ (K) |
|---|---|---|---|---|---|
| 0.07 | 460 | 0.78 | 18.0 | 3.6 | 18.2 |
| 0.10 | 220 | 0.35 | 28.2 | 1.7 | 28.5 |
| 0.12 | 230 | 0.28 | 33.7 | 1.5 | 33.7 |
| 0.14 | 270 | 0.19 | 38.9 | 0.5 | 38.9 |
| 0.15 | 150 | 0.22 | 31.6 | 1.8 | 32.1 |
| 0.16 | 140 | 0.12 | 35.5 | 1.6 | 35.9 |
| 0.17 | 140 | 0.15 | 34.4 | 1.7 | 34.7 |
| 0.17 | 115 | 0.14 | 34.4 | 1.2 | 34.7 |
| 0.18 | 240 | 0.11 | 34.5 | 1.3 | 34.8 |
| 0.18 | 120 | 0.15 | 27.9 | 2.7 | |
| 0.18 | 60 | 0.15 | 27.8 | 1.5 | 28.0 |
| 0.19 | 135 | 0.09 | 26.7 | 1.0 | 26.9 |
| 0.20 | 90 | 0.05 | 32.4 | 1.7 | 32.8 |

## III. EXPERIMENTAL

### A. High-quality LSCO films

Epitaxial LSCO thin films covering a wide range from $x=0.07$ to 0.20 were grown on $LaSrAlO_4$ (001) substrates by a pulsed laser deposition technique. Details of the growth condition were described elsewhere.[31–33] Pure ozone in an atmosphere of 10 mPa was used for oxidation during both the deposition and post-annealing processes in the growth chamber, in order to obtain superconducting LSCO films with very low residual resistivity. The excellent $c$-axis orientation of each film was confirmed by x-ray diffraction. The rocking curve of the 002 reflection showed the full width at half maximum (FWHM) of about 0.2°, which was almost the same as FWHM of $LaSrAlO_4$ (LSAO) substrate, suggesting that the mosaicness of the film is not so much different from that of the substrate.[32]

All films were carefully annealed in air (or $O_2$ gas for $x=0.20$) at 700 °C for 2–4 hours, following the heat treatment procedure developed for high-quality LSCO single crystals.[34] The annealed samples were rapidly quenched down to low temperatures using liquid nitrogen.

The in-plane dc resistivity, $\rho_{\rm dc}$, of each film was measured using a standard four-probe method. Table I lists a thickness,

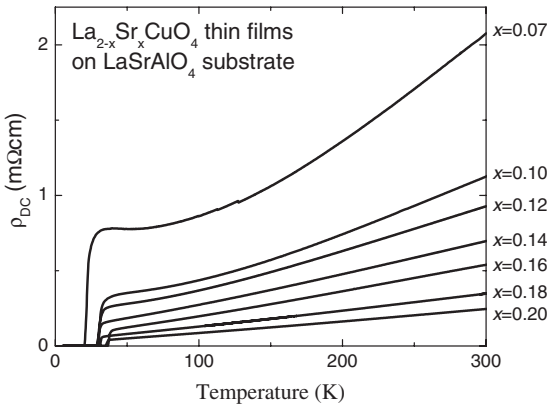


FIG. 1. Temperature dependence of the dc resistivity for LSCO thin films with $x=0.07-0.20$.

the resistivity at $T=50$ K, $T_c$ defined by zero resistance, $\Delta T_c$ defined by the 10%–90% transition width, and $T_c$ used in the dynamic scaling analysis for all the samples. As shown in Fig. 1 and Table I, we confirmed that the absolute value of $\rho_{dc}$ just above $T_c$ systematically decreased with increasing hole doping within the experimental error and also that it agreed with the reported best values for LSCO thin films[35,36] and single crystals[37] with the same value of $x$ within the factor of 2. Note that such a factor of 2 does not influence the critical phenomenon in the vicinity of $T_c$ as a function of the Sr concentration. In the present study, we used commercially available LSAO substrates with no special treatment to the surface condition. Thus, the crystallographic quality of the heteroepitaxially grown LSCO thin films is not necessarily identical since it is affected by the surface condition of the substrate. However, such a crystallographic imperfection occurs in an atomic scale, which can be safely neglected in a much larger scale of the coherence length in the vicinity of $T_c$.

Together with the narrow rocking curve observed by the x-ray diffraction, these properties show that the thin films under this study are of so high quality that the critical phenomenon near $T_c$ deserved to be investigated experimentally. Note that the transitions appear to be broad, especially for underdoped films. However, this is a consequence of the fluctuation and is not due to the inhomogeneity of $T_c$. The only exception is the 120 nm thick film with $x=0.18$, which will be referred in Sec. V as an example of the breakdown of the dynamics scaling due to the inhomogeneity of $T_c$.

As was already described in our previous paper,[20] for the purpose of investigating the critical charge dynamics in a whole region of the phase diagram, LSCO is an ideal system with a simple layered structure, where the hole concentration can be widely controlled. In addition, the use of LSAO substrate for LSCO films provides an advantage over bulk crystals of LSCO because the tetragonal symmetry of LSAO substrate prevents the corrugation in the $CuO_2$ plane, which is attributed to a staggered rotation of $CuO_6$ octahedra in low-temperature orthorhombic (LTO) phase of bulk LSCO.[32] Thus, we can expect that ideal flat square $CuO_2$ planes, which are free from disorders due to corrugations and twin boundaries, are realized in LSCO films on LSAO substrate.

### B. Microwave broadband technique

When the film thickness, $t$, is sufficiently smaller than the skin depth, $\delta$, the frequency-dependent microwave complex conductivity, $\sigma(\omega)$, can be obtained from the complex reflection coefficient, $S_{11}(\omega)$, as follows:[38]

$$\sigma(\omega) = \frac{1}{tZ_0}\frac{1-S_{11}(\omega)}{1+S_{11}(\omega)}, \tag{6}$$

where $t$ and $Z_0(=377\ \Omega)$ are the film thickness and the impedance of free space, respectively.

We measured the frequency dependence of $S_{11}(\omega)$ in the frequency range between 45 MHz and 10 GHz by using a vector network analyzer (HP 8510C) in a step-sweep mode. The thin-film sample with the electrodes in a Corbino disk shape was terminated to the end of a coaxial cable through a modified jack-to-jack coaxial adaptor. The contact electrodes of LSCO thin films in the Corbino disk geometry were formed by painting ink with gold nanoparticles (Au nanometal ink, ULVAC Materials Inc.). After painting, they were dried on a hot plate at 200 °C for several minutes and annealed in $O_2$ gas (or air for $x=0.07$) at 800 °C for 3 min. The contact resistance in these electrodes was estimated about 10 mΩ from a residual resistance in the superconducting state, independently of $x$. We found that this was the best way to obtain the smallest contact resistance among the methods we tried (for instance, a standard gold sputtering or a gold evaporation). The contact electrodes formed by this method were very durable so that we could repeat the $S_{11}(\omega)$ measurements for the same sample.

A stable electrical contact between the sample and the modified coaxial adaptor was realized by two springs, following the work by Booth *et al.*[39] One spring was embedded into a center conductor pin of the adaptor and the other spring was located at the backside of the LSAO substrate. Other details of the experimental setup are described elsewhere.[40]

In practice, the measured reflection coefficient, $S_{11}^{meas}(\omega)$, is affected by the attenuation and the phase shifts in the intervening coaxial cable, giving rise to large systematic errors at lower temperatures and higher frequencies. Thus, $S_{11}^{meas}(\omega)$ is given by the following equation:[41]

$$S_{11}^{meas}(\omega) = E_D(\omega) + \frac{E_R(\omega)S_{11}(\omega)}{1-E_S(\omega)S_{11}(\omega)}, \tag{7}$$

where, $E_D(\omega)$, $E_R(\omega)$, and $E_S(\omega)$ are complex error coefficients, representing the directivity, the reflection tracking, and the source mismatching, respectively. A standard method to determine these unknown error coefficients is to measure three known reference samples as a function of frequency at each temperature. Typically, we used a gold film as a short standard, a NiCr film as a load standard, and a teflon sheet as an open standard, following the work by Stutzman *et al.*[42] By performing this standard calibration procedure, both $\sigma_1(\omega)$ and $\sigma_2(\omega)$ for all LSCO films were successfully obtained in the frequency range at least between 0.1 and 10 GHz, as shown in Fig. 2. For all films, we confirmed that the skin depth $\delta$ at 10 GHz, which was given by $\sigma(\omega)$, was sufficiently longer than the film thickness $t$ over the whole mea-

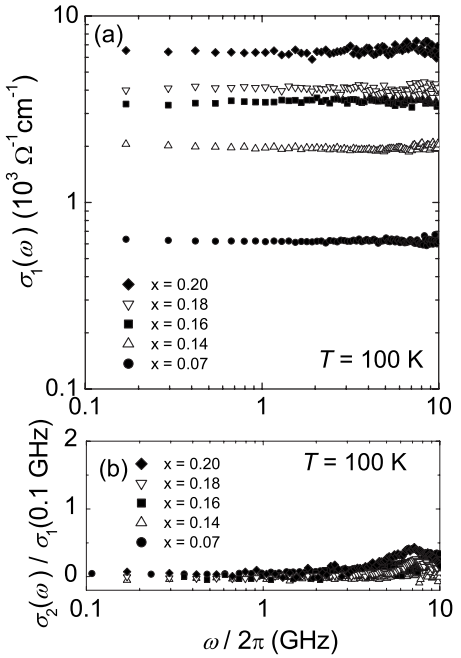


FIG. 2. (a) Frequency dependence of $\sigma_1$ for LSCO thin films with $x=0.07-0.20$ at $T=100$ K. (b) Frequency dependence of $\sigma_2$ normalized by $\sigma_1$ at 0.1 GHz for the same films. For all films, $\sigma_1$ is independent of frequency and $\sigma_2$ is much smaller than $\sigma_1$, suggesting that the charge dynamics in the normal state can be safely regarded as in the Hagen-Rubens limit of the Drude conductivity.

sured temperature range including the vicinity of $T_c$ and that the frequency dependence of both $\sigma_1(\omega)$ and $\sigma_2(\omega)$ well above $T_c$ could be regarded as those in the Hagen-Rubens limit of the Drude conductivity.[38]

### C. Calibration procedure to obtain complex fluctuation conductivity

The standard calibration procedure using three known standards is based on the high reproducibility between four measurements including three known reference samples and an unknown LSCO sample. In our measurement apparatus, the measured $S_{11}$ was reproduced typically within 0.05 dB in the magnitude and 0.2° in the phase of $S_{11}$ at 1 GHz. As shown in Fig. 2, this reproducibility was enough for us to obtain $\sigma(\omega)$ between 0.1 and 10 GHz for LSCO films far above $T_c$. However, as was already reported by our previous paper,[20] we found that the present reproducibility was insufficient to obtain $\sigma(\omega)$ in the vicinity of $T_c$. This is because a small unexpected difference between the phase of $S_{11}^{\text{short}}$ and that of $S_{11}^{\text{load}}$ gave rise to a large error in $\sigma(\omega)$ in the vicinity of $T_c$, as suggested by Eq. (6).

In order to overcome this difficulty, we modified the calibration procedure as follows. First of all, we regarded both the magnitude and phase parts of $S_{11}(\omega)$ for the LSCO sample, which were measured at a temperature ($T=T_0$) well above $T_c$, as those of $S_{11}^{\text{load}}$, based on the observation that the normal-state conductivity of the LSCO films was regarded as that in the Hagen-Rubens limit of the Drude conductivity. Next, we equated the phase of $S_{11}^{\text{short}}$ to that of $S_{11}^{\text{load}}$ at $T=T_0$

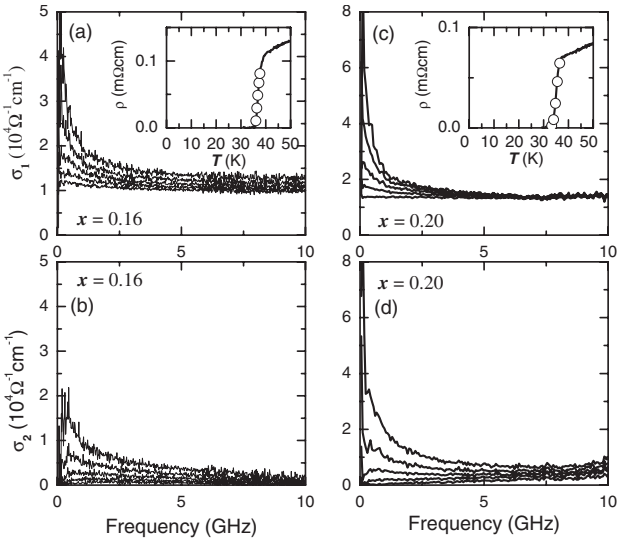


FIG. 3. Frequency dependence of (a) $\sigma_1$ and (b) $\sigma_2$ of the $x=0.16$ film at $T=36.0-37.6$ K and (c) $\sigma_1$ and (d) $\sigma_2$ for the $x=0.20$ film at $T=33.2-36.5$ K. All temperatures are just above $T_c$. Both $\sigma_1$ and $\sigma_2$ showed a remarkable enhancement in the low-frequency limit as temperature approaches $T_c$. Insets show the temperature dependence of dc resistivity. Each circle represents the temperature of each data in the main panels.

based on the assumption that a small difference between them was purely due to the experimental error. Finally, we assumed that the phase parts of both $S_{11}^{\text{short}}$ and $S_{11}^{\text{load}}$ were independent of temperature in a narrow range between $T_c$ and $T_0$. Thus, the phase of $S_{11}^{\text{short}}$ agreed with that of $S_{11}^{\text{load}}$ at any temperature from $T_c$ to $T_0$, as expected for the ideal load and short standards. We also confirmed the validity of this procedure by the same measurements of conventional NbN superconducting thin films as a reference.[24]

If $\sigma(\omega)$ was obtained at each temperature in the vicinity of $T_c$ through the modified calibration procedure, the complex fluctuation conductivity, $\sigma_{\text{fl}}(\omega,T)$, is given by the following equation:

$$\sigma_{\text{fl}}(\omega,T) \equiv \sigma(\omega,T) - \sigma_n(T). \tag{8}$$

Here, $\sigma_n(T)$ is the normal-state component included in $\sigma(\omega,T)$, which agrees with the normal-state conductivity far above $T_c$. Although the change of $\sigma_n(T)$ with decreasing temperature was estimated by the linear extrapolation of dc conductivity from higher temperatures, we found that the dynamic scaling behavior of the extracted $\sigma_{\text{fl}}(\omega)$ in the vicinity of $T_c$ was insensitive to the temperature dependence of $\sigma_n(T)$.

## IV. RESULTS

### A. Doping dependence in zero magnetic field

Figure 3 shows the typical frequency dependence of $\sigma(\omega)$ for the optimally doped LSCO ($x=0.16$) and the overdoped LSCO ($x=0.20$) at several temperatures near $T_c$ in zero magnetic field. We observed that both $\sigma_1(\omega)$ and $\sigma_2(\omega)$ in the low-frequency limit diverged rapidly as the temperature ap-

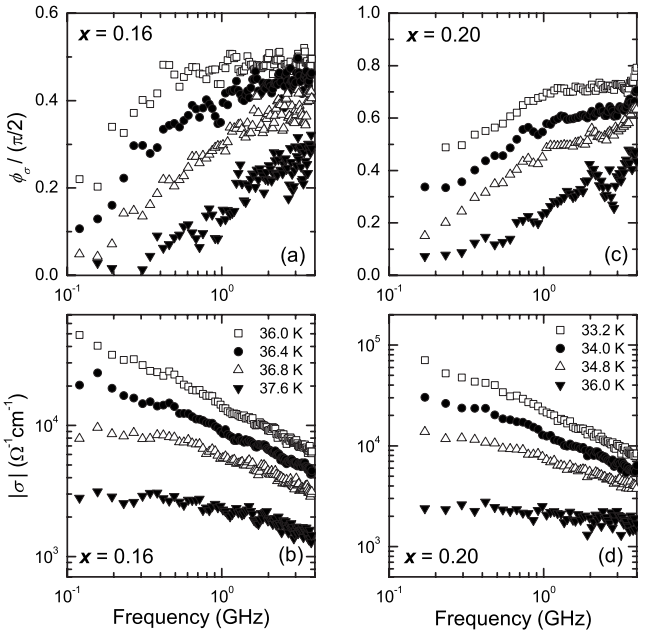


FIG. 4. Frequency dependence of (a) the phase, $\phi_\sigma$, and (b) the magnitude, $|\sigma|$, of the fluctuation-induced complex conductivity for the $x=0.16$ film and (c) $\phi_\sigma$ and (d) $|\sigma|$ for the $x=0.20$ film.

proached $T_c$ from above, suggesting that the contribution of the superconducting fluctuations to $\sigma(\omega)$ was evident with decreasing temperature. This behavior was more clearly demonstrated by plotting the phase and the magnitude of $\sigma_{\rm fl}(\omega)(=\sigma(\omega)-\sigma_n)$ as a function of frequency. Figures 4(a) and 4(c) show that the plots of the dimensionless phase angle, $\phi_\sigma$, of $\sigma_{\rm fl}$ versus frequency move to a lower frequency region with decreasing temperature, suggesting that a characteristic time scale of the superconducting fluctuations is critically slowing down. On the other hand, as shown in Figs. 4(b) and 4(d), the magnitude, $|\sigma|$, of $\sigma_{\rm fl}$ increases rapidly with decreasing temperature, suggesting a critical divergence of the superconducting fluctuations.

Following the scaling procedures described in Sec. II, we tested whether these behaviors were truly attributed to the critical fluctuations of the superconducting order or not. Figure 5 shows the results of the data scaling of $\phi_\sigma$ (upper panels) and $|\sigma_{\rm fl}|$ (lower panels) for the LSCO films with five Sr concentrations from $x=0.15$ to $x=0.20$. As clearly indicated in Fig. 5, we confirmed that both of $\phi_\sigma$ and $|\sigma|$ successfully collapsed on to single curves for all Sr concentrations, strongly suggesting that the dynamic scaling hypothesis was successfully satisfied so that we could investigate the change of the critical behavior as a function of the Sr concentration along this line.

The solid and dashed lines depicted in Fig. 5 were the 2D and 3D Gaussian scaling functions, respectively, which were calculated by Schmidt.[43] They play roles of the guide to eyes for the dimensionality in the critical charge dynamics, suggested by Eqs. (4) and (5). We found that the optimally doped LSCO ($x=0.15, 0.16$) showed the 3D-like critical behavior while the overdoped LSCO ($x=0.18\sim0.20$) showed the 2D-like critical behavior.[44] This suggestion was quantitatively confirmed by the plots of the scaling parameters, $\omega_0$ and $\sigma_0$, versus the reduced temperature, $T/T_c-1$, as shown in Fig. 6. Here, we used the values of $T_c^{\rm scale}$ as $T_c$. The error bars on the scaling parameters were estimated by using the methods described in the Appendix. In the dynamic scaling theory by FFH,[19] the plots of $\omega_0\sigma_0(\propto\xi^{2-d})$ are expected to be independent of $T/T_c-1$ for $d=2$, while they are expected to increase monotonously with $T/T_c-1$ for $d=3$. It should be noted that these behaviors are not affected by the ambiguity of $T_c^{\rm scale}$. Thus, within the error bars of $\omega_0\sigma_0$, Figs. 6(a) and 6(d) clearly indicate that the dimensional crossover from 3D

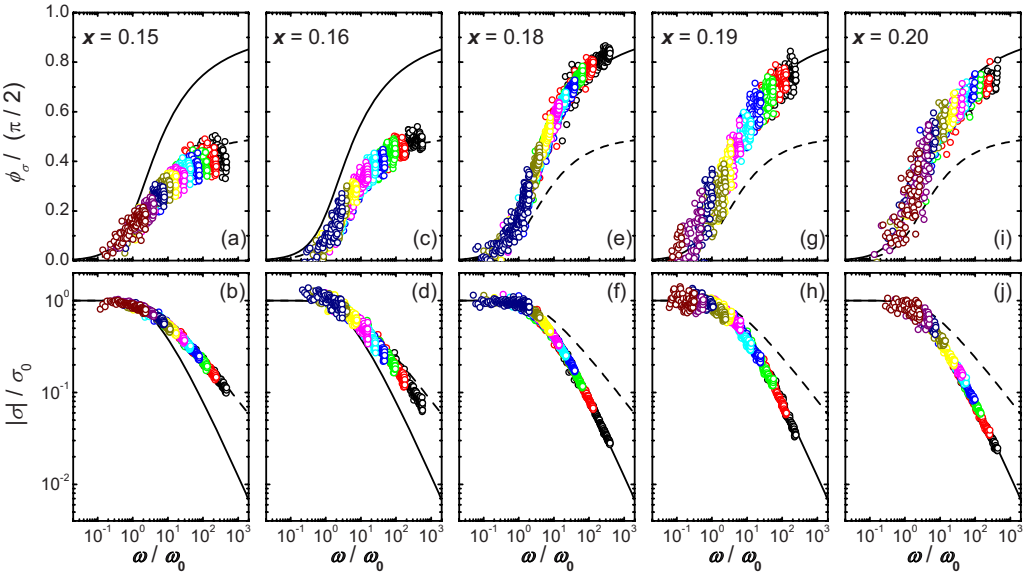


FIG. 5. (Color online) Scaled data of the phase (upper panels) and the magnitude (lower panes) of $\sigma_{{\rm fl}(\omega)}$ for the LSCO films with various carrier concentrations. The phase and the magnitude are normalized by $\pi/2$ and the scaling parameter, $\sigma_0$, respectively. Difference in colors represents the measured data at different temperatures. The temperature ranges of the scaled data for each film are from $T=32.4$ to 35.0 K($x=0.15$), from $T=36.0$ to 37.6 K($x=0.16$), from $T=28.2$ to 31.0 K($x=0.18$), from $T=27.0$ to 29.0 K($x=0.19$), and from $T=33.2$ to 36.5 K($x=0.20$), respectively. Solid (dashed) lines are the 2D (3D) Gaussian scaling functions.

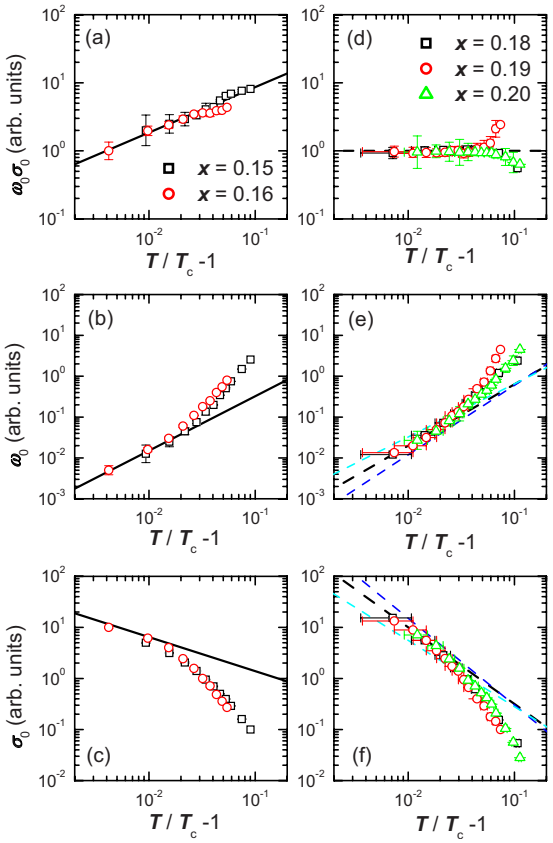


FIG. 6. (Color online) Temperature dependence of the obtained scaling parameters: $\omega_0\sigma_0$ (top), $\omega_0$ (middle), and $\sigma_0$ (bottom). Left (Right) panels are for the optimally doped (the overdoped) LSCO. Error bars along the vertical and horizontal directions were estimated by the methods described in the Appendix and by the ambiguity of $T_c^{\rm scale}$, respectively. Solid lines in the left panels are calculations given by Eqs. (2) and (3) with $\nu=0.67$, $z=2$, and $d=3$, suggesting the 3D-*XY* critical charge dynamics. Three dashed lines in the right panels are similar calculations with $d=2$ and $\nu z=1.3, 1.5, 1.7$, respectively.

to 2D occurred near the boundary between the optimally doped region and the overdoped region.

As was already described in Sec. II, the ambiguity of $T_c^{\rm scale}$ affects the values of $\nu$ and $z$, when we determine them from the temperature dependence of $\omega_0$ and $\sigma_0$. Qualitatively, $T_c^{\rm scale}$ must be larger than $T_c^R$ and be smaller than the minimum temperature down to which $\phi_\sigma$ and $|\sigma|$ are successfully scaled on to single curves. With any value of $T_c^{\rm scale}$ within this range, we confirmed that $\omega_0$ and $\sigma_0$ for the optimally doped LSCO with $x=0.15$ and $x=0.16$ agreed with those for the relaxational 3D-*XY* universality class with $\nu=0.67$ and $z\approx 2$ (Ref. 45) rather than those for the 3D Gaussian fluctuation whose critical exponents are $\nu=0.5$ and $z=2$. As shown in Figs. 6(b) and 6(c), we also estimated the error bars of $T_c^{\rm scale}$ for the optimally doped LSCO with $x=0.15$ and $x=0.16$, which were found to be less than 0.05 K by using the linear plots of the $\nu$th root ($\nu=0.67$) of $\omega_0\sigma_0$ versus temperature.

On the other hand, $\omega_0$ and $\sigma_0$ for the overdoped LSCO with $x=0.18-0.20$ were found neither to show an exponential singularity expected for the 2D-*XY* universality class nor

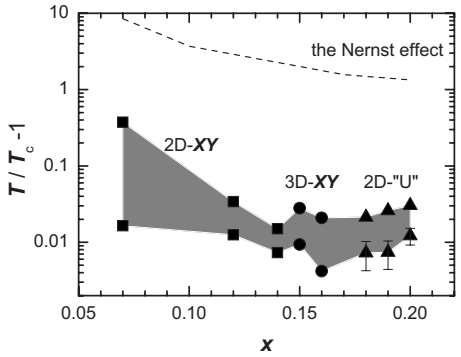


FIG. 7. Plots of the highest (or the lowest) temperatures where one of the possible universality classes was clearly observed as a function of the Sr concentration (hatched area). Difference in symbols represents the difference in the observed critical behavior, which is classified into three groups of 2D-*XY* (squares), 3D-*XY* (circles), and 2D-"U" (triangles). Below the dashed line, the Nernst signal was observed (Ref. 49).

to show a divergence with an exponent of $\nu z=1$ for the 2D Gaussian fluctuation. Rather, they seemed to show a divergence with an unusual exponent of $\nu z=1.5\pm 0.2$, as shown in Figs. 6(e) and 6(f). Here, the error bars on $\nu z$ were estimated by considering the ambiguity of $T_c^{\rm scale}$, which was typically less than 0.1 K. Note that a lower value of $T_c^{\rm scale}$ closer to $T_c^R$ can provide a larger value of $\nu z$ exceeding 2, where the temperature dependence of $\omega_0$ and $\sigma_0$ seems to be described by a single power law up to higher temperatures. However, we considered that the value of $\nu z$ exceeding 2 was an overestimation, since the so-called short-wavelength cutoff effect should be considered at higher temperatures far from $T_c$, as was previously reported by Johnson *et al.*[46] The critical behavior with $\nu z=1.5\pm 0.2$ observed for the overdoped LSCO shows a sharp contrast to the behavior for the underdoped LSCO with $x=0.07-0.14$, as already reported in the previous paper.[20] We note that this is never explained by the known universality class, such as the 2D-*XY* or Gaussian fluctuations. Thus, we refer this unusual behavior to the 2D-"U" as an unknown universality class. In the next section, we discuss the origin of this unusual behavior in terms of various possible candidates.

Figure 7 shows a summary of our results about the critical charge dynamics of LSCO as a function of the Sr concentration. The temperature region where the suggested universality class became dominant was determined by fitting of the temperature dependence of $\omega_0$ to corresponding models. Together with our previous study for the underdoped LSCO,[20] we found that two kinds of the sudden dimensional crossovers took place across the phase diagram. One is the dimensional crossover from 2D-*XY* to 3D-*XY* between $x=0.14$ and $x=0.15$, while the other is the dimensional crossover from 3D-*XY* to 2D-"U" between $x=0.16$ and $x=0.18$. The first dimensional crossover was already reported in our previous study,[20] while the second was observed by this work. In the following two sections, we first investigate the critical behavior in the overdoped LSCO in more detail in terms of finite-size effects.

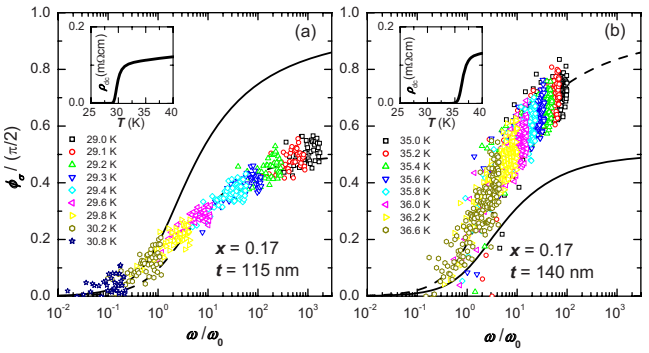


FIG. 8. (Color online) Scaled data of $\phi_\sigma$ for the $x=0.17$ films with different thicknesses. They are plotted in a temperature range from $T=29.0$ to 30.8 K for the $t=115$ nm film and from $T=35.0$ to 36.6 K for the $t=140$ nm film. Solid (dashed) lines are the 2D (3D) Gaussian scaling function. Insets: Temperature dependence of dc resistivity of the corresponding films.

### B. Finite-size effect

In this study, we used relatively thin LSCO films in the overdoped regime, as listed in Table I. This is because, for the reliable data of $\sigma_{fl}(\omega)$ to be obtained by the microwave broadband technique, the sheet resistance just above $T_c$ is needed to be larger than about 2 $\Omega$. This condition requires us to use thinner films for less resistive overdoped LSCO. However, the use of thinner films leads to a suspicion that the observed 2D-like critical behavior for the overdoped LSCO is caused by a finite film thickness. Indeed, we have demonstrated that the dynamic fluctuations in the superconducting NbN thin films showed the 2D Gaussian fluctuations, which were introduced by the divergence of $\xi$ beyond the film thickness.[24]

In order to investigate this problem, we measured the films with different thickness near the Sr concentration where the second dimensional crossover occurred. Figures 8 and 9 show the scaled data of $\phi_\sigma$ for $x=0.17(t=115,140$ nm) and $x=0.18(t=60,240$ nm), respectively.

First of all, as shown in Fig. 8, the behavior of $\phi_\sigma(\omega)$ scaled by $\omega_0$ for $x=0.17$ showed the 2D-like behavior for the thicker film ($t=140$ nm) and the 3D-like behavior for the thinner film ($t=115$ nm). It is clear that this change of the dimensionality cannot be explained by the finite-size effect, in contrast to the previous results on the NbN films.[24] Rather, this result implied a possibility that the intrinsic dimensional crossover occurs suddenly near $x=0.17$.

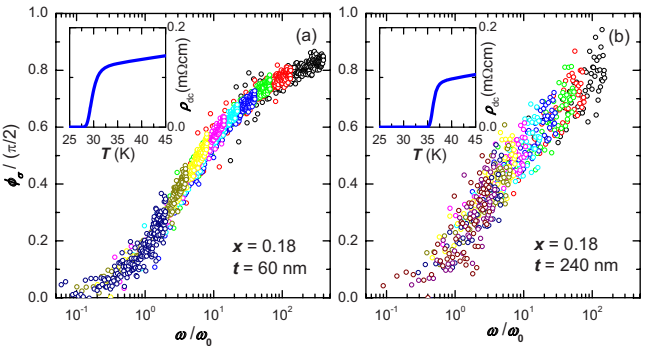


FIG. 9. (Color online) Scaled data of $\phi_\sigma$ for the $x=0.18$ films with (a) 60 nm thick and (b) 240 nm thick. They are plotted in a temperature range from $T=28.2$ to 31.0 K for the $t=60$ nm films and from $T=35.0$ to 37.0 K for the $t=240$ nm films. Insets: Temperature dependence of dc resistivity of the corresponding films.

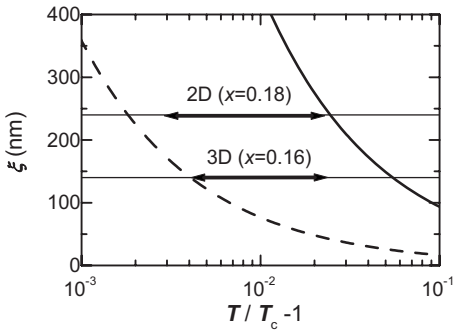


FIG. 10. Dashed (solid) thick line represents a critical divergence of $\xi(T)=\xi_0(T/T_c-1)^{0.67}$ in the 3D-$XY$ critical charge dynamics with $\xi_0=3.5$ nm(20 nm). Solid arrows show temperature ranges where the critical behavior was observed for the two LSCO ($x=0.16$ and $x=0.18$, respectively). Thin solid lines show the thicknesses, $t$, of the two films. Note that the 3D-$XY$ critical charge dynamics of the $x=0.16$ film was not cut off by the film thickness ($t=140$ nm) in the observed temperature range. This suggests that $\xi_0$ is smaller than 3.5 nm. On the other hand, if the 2D critical behavior of the $x=0.18$ film in the observed temperature range was attributed to the 3D-$XY$ critical behavior, which was cut off by the film thickness ($t=240$ nm), $\xi_0$ must be larger than 20 nm.

The behaviors of $\phi_\sigma$ for $x=0.18$ agreed with the 2D-like critical charge dynamics even for the thicker film ($t=240$ nm), as shown in Fig. 9. By comparing this result to that of the film with $x=0.16(t=140$ nm) which showed the 3D-$XY$ critical charge dynamics, it provided us the following important insight. As shown in Fig. 10, the 2D-like critical fluctuations for the thicker film could be observed in the temperature range from $(1.006\pm0.003)T_c$ to 1.02 $T_c$ by considering the ambiguity of $T_c^{\text{scale}}$. If we consider that the 2D behavior is due to the finite-thickness effect on the 3D-$XY$ critical behavior, $\xi$ should be larger than the film thickness ($t=240$ nm) below 1.02 $T_c$. This requires that $\xi_0$ is larger than 20 nm. On the other hand, the 3D-$XY$ fluctuations for $x=0.16$ were observed in the temperature range from 1.004 $T_c$ to 1.02 $T_c$. This means that $\xi(T)$ is not larger than $t=140$ nm above $T=1.004$ $T_c$, requiring that $\xi_0$ is less than 3.5 nm. Note that such estimations of $\xi$ are not influenced by the ambiguity of $T_c^{\text{scale}}$, since it becomes more important only for $x=0.18$ in the vicinity of $T_c$ as suggested by Fig. 6. Thus, a difference of $\xi_0$ between $x=0.16$ and $x=0.18$ needs to be larger than 6 times in magnitude. This seems to be too large to be explained by the change of $T_c$ or the superconducting gap with hole doping. Therefore, the observed behaviors in $\phi_\sigma$ for these films with different thickness never supported that the 2D-like critical behavior near $x=0.18$ was attributed to the finite-thickness effect. The same conclusion was also obtained from the scaled data of $|\sigma|$.

### C. Effects of external magnetic field

Another way to investigate a finite-size effect in the critical charge dynamics is the use of an external magnetic field

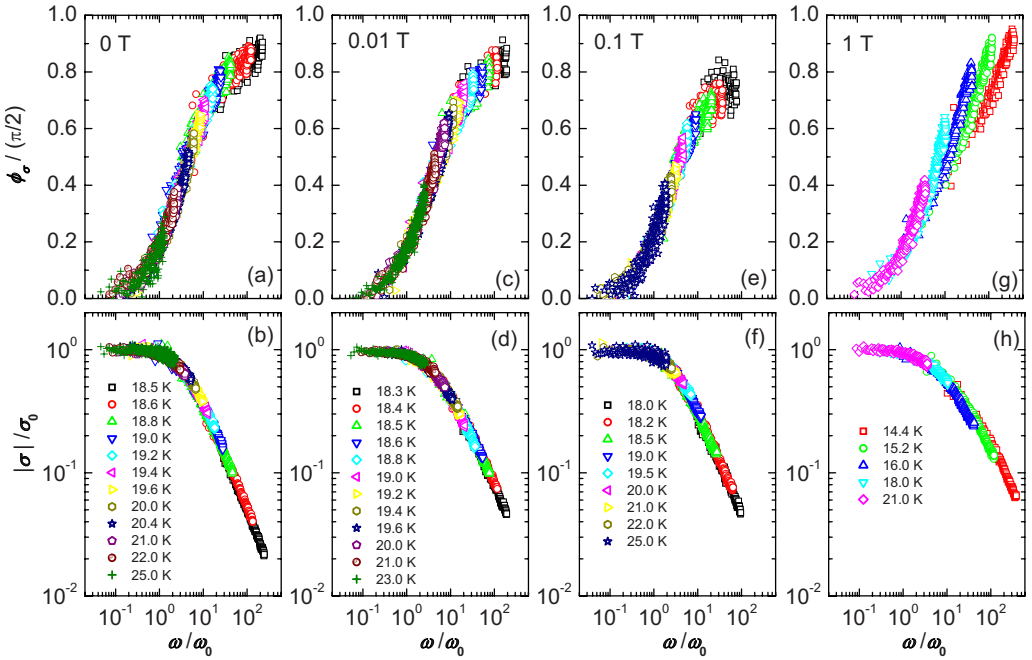


FIG. 11. (Color online) Scaled data of $\phi_\sigma$ (upper panels) and $|\sigma|$ (lower panes) for the $x=0.07$ film in zero and finite magnetic fields.

perpendicular to the film. If a magnetic field larger than the lower critical field was applied to a type-II superconductor, vortices can penetrate into the superconductor. Since the vortex pinning effect is negligibly small near $T_c$, vortices are distributed uniformly over the sample. At the core of each vortex, the growth of the superconducting order parameter is strongly suppressed, suggesting the divergence of $\xi$ due to the superconducting fluctuation is cut off by a finite distance between vortices. Thus, the external magnetic field can be used as a tunable probe to study the finite-size effect, since the mean distance between vortices, $\ell_v$, is proportional to $\sqrt{\Phi_0/B}$.

Of course, it is crucially important to distinguish the critical charge dynamics under a magnetic field from the vortex dynamics in the mixed state. For this purpose, we measured four LSCO films ($x=0.07$, 0.16, 0.17, and 0.18) by applying magnetic field perpendicular to the $CuO_2$ planes up to 1 T systematically and investigated the obtained results very carefully.

Figure 11 shows the scaled data of $\phi_\sigma$ and $|\sigma|$ for the underdoped LSCO ($x=0.07$) at several constant magnetic fields. We found that both $\phi_\sigma$ and $|\sigma|$ were scaled successfully up to $B=0.1$ T, while neither of them were collapsed on to single curves at $B=1$ T. This suggests that the contribution of the vortex dynamics is almost negligible up to at least $B=0.1$ T, whereas it cannot be neglected at $B=1$ T. As shown in Figs. 12(a) and 12(b), we confirmed again that the behavior of $\omega_0$ and $\sigma_0$ obtained at $B=0$ T excellently agreed with the BKT theory in the temperature range from $1.02T_c$ to $1.2T_c$. Note that $\omega_0^{-1} \propto \sigma_0 \propto \xi_{\mathrm{KT}}^2$ in the relaxational 2D-$XY$ universality class. Here, the BKT correlation length, $\xi_{\mathrm{KT}}$, shows an exponential divergence in a critical region, as follows:

$$\xi_{\mathrm{KT}} = \xi_0 \exp[b/\sqrt{T/T_c - 1}], \tag{9}$$

where $b$ is a numerical constant, which was determined to be $\sim 0.2$ in this study.

The plots of the correlation length, $\xi$, given by $1/\sqrt{\omega_0}$ as a function of $1/\sqrt{T/T_c - 1}$ were found to be very useful to understand the finite-size effect due to the external magnetic field. As is shown in Fig. 12(c), the divergence of $\xi$ in the vicinity of $T_c$ was suppressed with increasing magnetic field. This behavior can be understood by considering two kinds of the characteristic length scale: the BKT correlation length, $\xi_{\mathrm{KT}}$, and the mean distance between vortices, $\ell_v$. In the temperature region not very close to $T_c$, where $\xi_{\mathrm{KT}} \ll \ell_v$, the

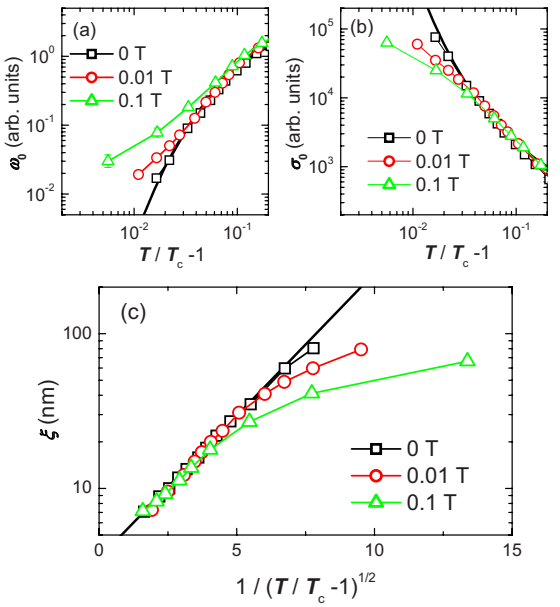


FIG. 12. (Color online) Temperature dependence of (a) $\omega_0$, (b) $\sigma_0$, and (c) $\xi \propto 1/\sqrt{\omega_0}$ for the $x=0.07$ film. Error bars of $\omega_0$, $\sigma_0$, and $\xi$ were estimated by using the methods described in the Appendix. Solid lines in each panel are calculations given by Eq. (9) with $\xi_0 = 3$ nm.

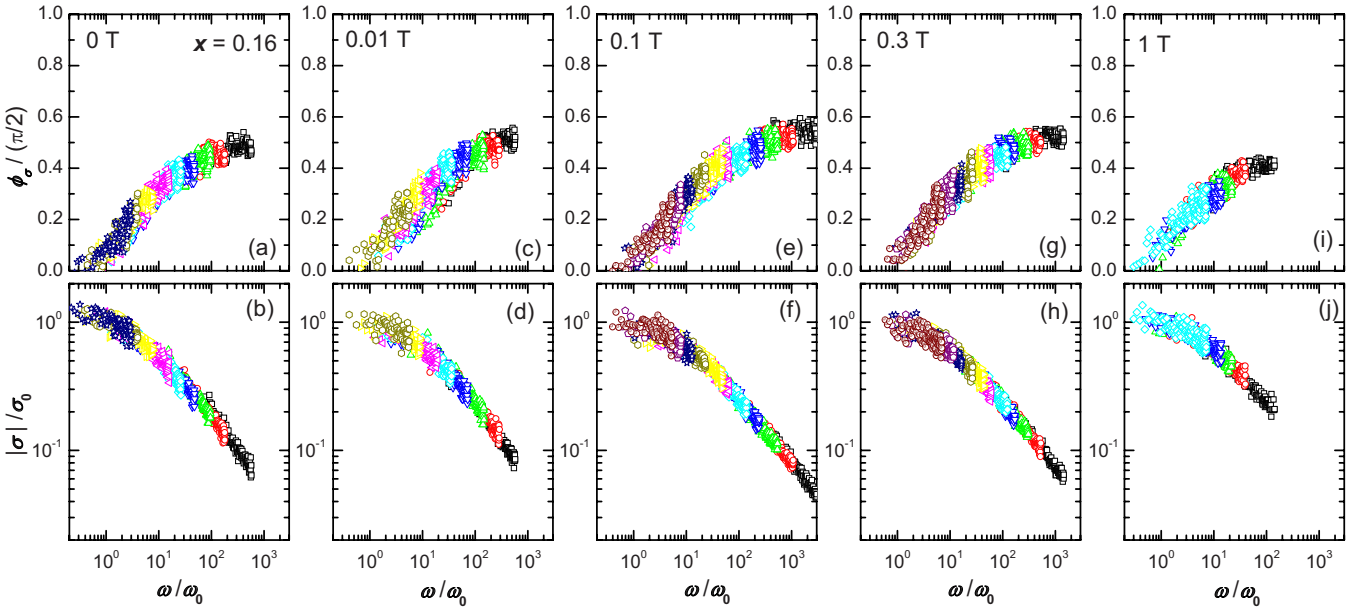


FIG. 13. (Color online) Scaled data of $\phi_\sigma$ (upper panels) and $|\sigma|$ (lower panes) for the $x=0.16$ film in zero and finite magnetic fields.

logarithmic interaction between a vortex and an antivortex, which is essential to the BKT transition, is not screened by the externally induced vortices. Thus, the exponential divergence due to $\xi_{\mathrm{KT}}$ is observed. On the other hand, in the vicinity of $T_c$, where $\xi_{\mathrm{KT}} \geq \ell_v$, the externally induced vortices can screen out the interaction between vortex and antivortex, leading to a crossover of the characteristic length scale from $\xi_{\mathrm{KT}}$ to $\ell_v$. Thus, the growth of $\xi$ is suppressed as $\xi$ approaches $\ell_v$. We confirmed that the saturated value of $\xi$ in the limit of $T_c$ did not exceed $\ell_v$ at each magnetic field by using a reasonable assumption that $\xi_0 \sim 3$ nm. In summary, the result of Fig. 12 is also consistent with the BKT picture for the fluctuation of the $x=0.07$ sample.

Figures 13 and 14 show the results of dynamic scaling analyses for the optimally doped LSCO ($x=0.16$) at several constant magnetic fields. We found that the data collapse of the scaled $\phi_\sigma$ and $|\sigma|$ to single curves were successful up to $B=1$ T, suggesting that the contribution of vortex dynamics was almost negligible in the measured magnetic field region. In addition, all the results clearly indicated that the 3D-*XY* critical charge dynamics was maintained up to $B=1$ T. Thus, the external magnetic field seemed not to give any change to the critical charge dynamics near $T_c$, in contrast to the case of the BKT transition. This is because the power-law-like divergence of $\xi(T)$ in the 3D-*XY* critical charge dynamics is much slower than the exponential divergence of $\xi_{\mathrm{KT}}(T)$. Indeed, by assuming that $\xi_0 \sim 3$ nm and $\nu=0.67$, we could estimate that $\xi(T)$ for this film ($x=0.16$) was less than 31 nm in the observed temperature range at $B=1$ T. Since $\ell_v$ is estimated to be $\sim 45$ nm at $B=1$ T, we can safely conclude that $\xi(T)$ is always smaller than $\ell_v$ even at $B=1$ T, strongly suggesting that the critical behavior is never affected by the external magnetic field at least up to $B=1$ T.

Figures 15 and 16 show the results of dynamic scaling analyses at several constant magnetic fields for the overdoped LSCO film ($x=0.18$ and $t=60$ nm). As was already pointed out, the critical charge dynamics of this film in zero magnetic field was represented by an unknown universality class in the 2D system (2D-"U"). Figure 15 clearly indicates that the scaled data of both $\phi_\sigma$ and $|\sigma|$ up to $B=1$ T were very similar to those at $B=0$ T. In addition, the temperature

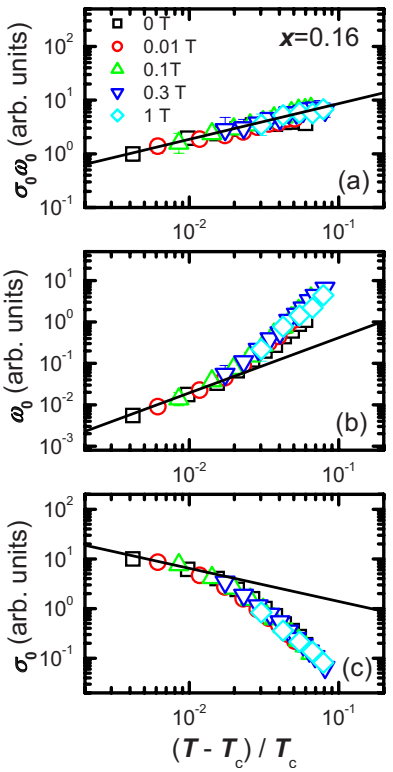


FIG. 14. (Color online) Temperature dependences of the obtained scaling parameters, (a) $\omega_0\sigma_0$, (b) $\omega_0$, and (c) $\sigma_0$, for the $x=0.16$ film in zero and finite magnetic fields. Error bars were estimated by using the methods described in the Appendix. Solid lines are calculations given by Eqs. (2) and (3) with $\nu=0.67$, $z=2$, and $d=3$, suggesting the 3D-*XY* critical charge dynamics.

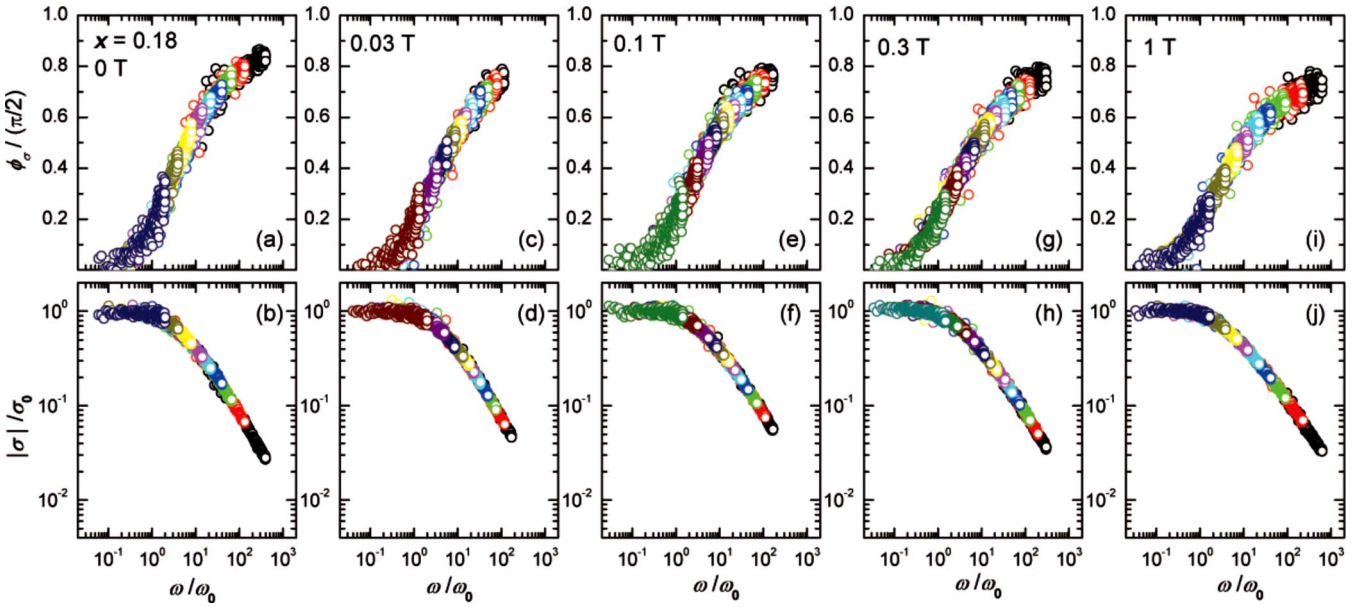


FIG. 15. (Color online) Scaled data of $\phi_\sigma$ (upper panels) and $|\sigma|$ (lower panes) for the $x=0.18$ film in zero and finite magnetic fields.

dependences of the scaling parameters at all magnetic fields except for $B=1$ T excellently agreed with each other, as shown in Fig. 16. These results strongly suggest that the small applied magnetic field (at least up to 0.3 T) did not affect the critical charge dynamics of the overdoped LSCO.

Thus, for both $x=0.16$ and $x=0.18$, the magnetic field dependence of the critical temperature, $T_c(B)$, which was experimentally determined through the dynamic scaling analysis at finite magnetic field below $B=0.3$ T, can be regarded as the same as the temperature dependence of the upper critical field, $B_{c2}(T)$, as shown in the inset of Fig. 17. Note that $B_{c2}$ is not a phase-transition point in practice. There is only a

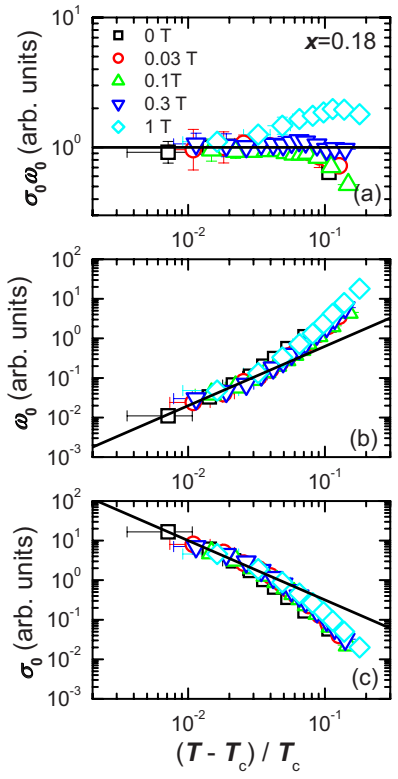


FIG. 16. (Color online) Temperature dependences of the obtained scaling parameters, (a) $\omega_0\sigma_0$, (b) $\omega_0$, and (c) $\sigma_0$, for the $x=0.18$ film in zero and finite magnetic fields. Error bars along the vertical and horizontal directions were estimated by the methods described in the Appendix and by the ambiguity of $T_c^{\rm scale}$, respectively. Solid lines are calculations given by Eqs. (2) and (3) with $\nu z=1.5$ and $d=2$.

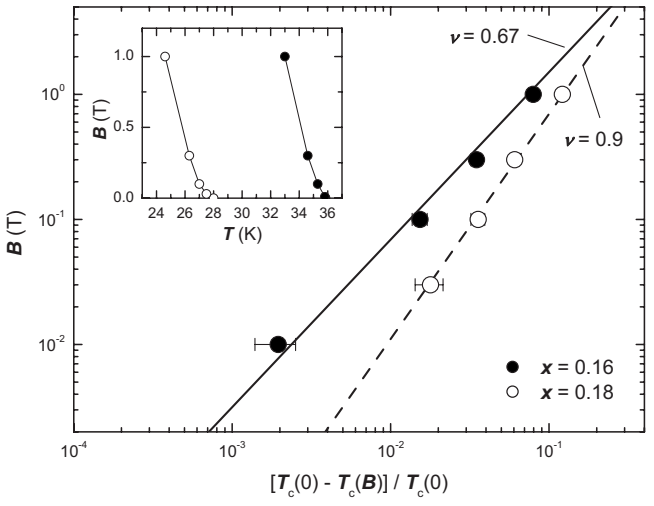


FIG. 17. Plots of the applied magnetic field for the optimally doped LSCO ($x=0.16$) and the overdoped LSCO ($x=0.18$) as a function of $1-T_c(B)/T_c(0)$. Error bars were estimated by the ambiguity of $T_c^{\rm scale}$. Solid and dashed lines are calculations given by Eq. (10) with $\nu=0.67$ and $\nu=0.9$, respectively. Inset: Plots of the applied magnetic field, $B$, as a function of the critical temperature, $T_c(B)$, for each film, which was determined through the dynamic scaling analysis at each magnetic field. If vortex dynamics can be neglected, this plot agrees with the temperature dependence of $B_{c2}(T)$.

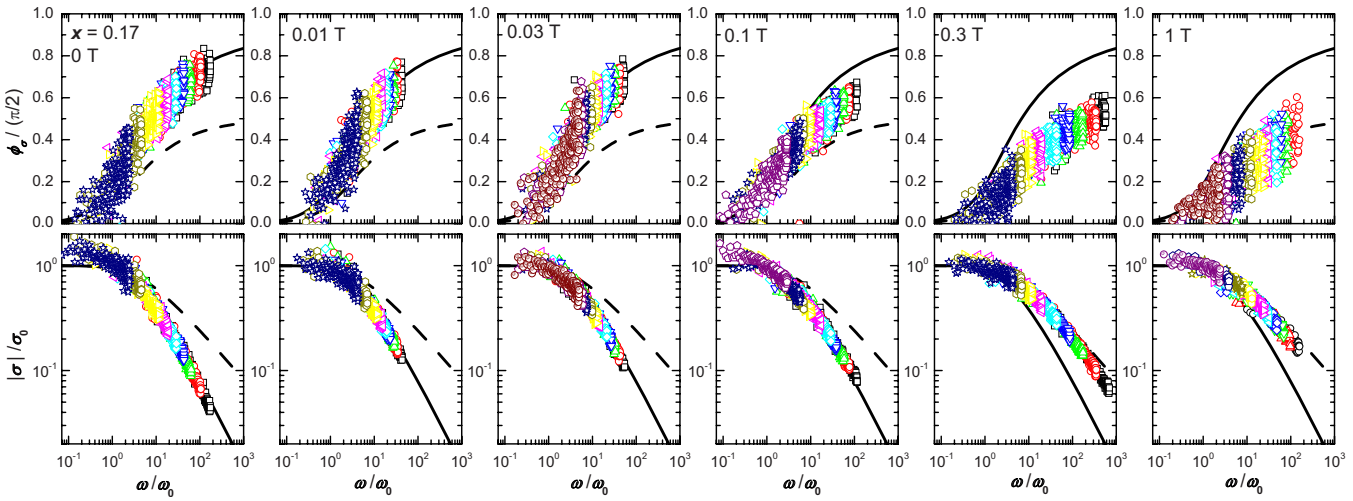


FIG. 18. (Color online) Scaled data of $\phi_\sigma$ (upper panels) and $|\sigma|$ (lower panels) for the $x=0.17$ film in zero and finite magnetic fields. Solid (dashed) lines are the 2D (3D) Gaussian scaling functions.

first-order transition of vortices at a lower field. However, the concept of $B_{c2}$ as the mean-field critical field still makes sense. This provides us another route to estimate $\nu$ and $\xi_0$ by using the following relationship:

$$B_{c2}(T) = \frac{\phi_0}{2\pi\xi(T)^2} = \frac{\phi_0}{2\pi}\frac{(1-T/T_{c0})^{2\nu}}{\xi_0^2}, \tag{10}$$

where $T_{c0}$ is the critical temperature at $B=0$ T. As shown in the main panel of Fig. 17, we confirmed that the plots of the applied magnetic field, $B$, as a function of $[1-T_c(B)/T_{c0}]$ for the optimally doped LSCO ($x=0.16$), agreed with a line of $B_{c2}(T)=\phi_0/2\pi\xi(T)^2$, with $\nu=0.67$ and $\xi_0\sim 3$ nm, as suggested by the dynamic scaling analyses for $x=0.16$. This supports the idea that the plots of $B$ as a function of $[1-T_c(B)/T_{c0}]$ can be regarded as those of $B_{c2}(T)$ as a function of $(1-T/T_{c0})$.

Based on this idea, we estimated that $\nu=0.9\pm0.05$ and $\xi_0\sim 3$ nm for the overdoped LSCO ($x=0.18$). Here, the error bars on $\nu$ were estimated by considering the ambiguity of $T_c^{\rm scale}$. As shown in Fig. 17, it is clear that the value of $\nu$ for $x=0.18$ is larger than the values for the Ginzburg-Landau (GL) theory ($\nu_{\rm GL}=0.5$) and the 3D-*XY* universality class ($\nu_{\rm 3DXY}=0.67$). We found that $\xi(T)$ increased up to 70 nm in the measured temperature range at $B=0.3$ T by using the estimated values of $\nu$ and $\xi_0$. Since $\ell_v$ was estimated as 83 nm at $B=0.3$ T, $\xi$ was always smaller than $\ell_v$ within the measured temperature range at least up to $B=0.3$ T, which confirmed that the critical charge dynamics, not the vortex dynamics, was observed. Together with the value of $\nu z(=1.5\pm0.2)$ obtained at $B=0$ T, we obtained that $z=1.7\pm0.3$ for $x=0.18$. Thus, the experimental results for $x=0.18$ suggested that the 2D-"U" universality class had the critical exponents of $\nu=0.9\pm0.05$ and $z=1.7\pm0.3$.

In contrast to the results for $x=0.16$ and 0.18, the behavior of $\phi_\sigma$ and $|\sigma|$ for $x=0.17$ (the thicker film, $t=140$ nm) was largely dependent on the applied magnetic field. Up to 0.1 T, the scaled data of $\phi_\sigma$ and $|\sigma|$ and the temperature dependences of the scaling parameters were similar to those at $B=0$ T, as shown in Figs. 18 and 19, respectively. By assuming that $\xi_0$ was about 3 nm, which was the same value as those used for $x=0.16$ and 0.18, $\xi(T)$ at 1.02 $T_c$ was estimated to be $\sim$100 nm for the 2D-"U" critical charge dynamics. Since $\ell_v$ was about 140 nm at $B=0.1$ T, $\xi(T)$ did not exceed $\ell_v$ up to $B=0.1$ T. Thus we confirmed that the con-

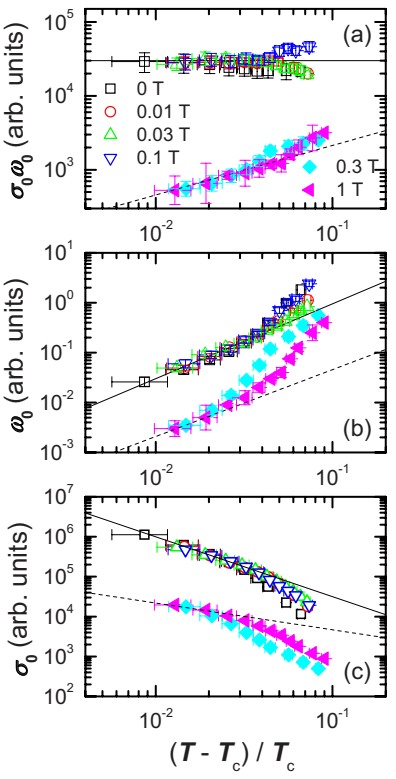


FIG. 19. (Color online) Temperature dependences of the obtained scaling parameters, (a) $\omega_0\sigma_0$, (b) $\omega_0$, and (c) $\sigma_0$, for the $x=0.17$ film in zero and finite magnetic fields. Error bars along the vertical and horizontal directions were estimated by the methods described in the Appendix and by the ambiguity of $T_c^{\rm scale}$, respectively. Solid (dashed) lines are calculations given by Eqs. (2) and (3) with $\nu z=1.5$ and $d=2$ ($\nu=0.67$, $z=2$, and $d=3$).

tribution of vortex dynamics was negligible and that the 2D-"U" critical charge dynamics retained up to 0.1 T. However, above 0.3 T, we found that the values of $\phi_\sigma(\omega/\omega_0)$ in the high-frequency limit clearly decreased with increasing magnetic field and also that the frequency dependence of $|\sigma(\omega/\omega_0)|$ was weakened, as shown in Fig. 18. Within the dynamic scaling theory,[19,22] these results seem to suggest that the dimensionality in the critical charge dynamics changes from 2D to 3D by applying magnetic field. Figure 19 also shows that the temperature dependence of $\sigma_0\omega_0(\propto\xi^{2-d})$ was changed markedly to the 3D-like above 0.3 T. However, we could not clearly confirm the 3D-*XY* critical charge dynamics since $\omega_0$ and $\sigma_0$ could be fitted by the critical exponents of the 3D-*XY* universality class only in a very narrow region between 1.01 $T_c$ and 1.03 $T_c$. This suggests a possibility that another contribution affects the critical behavior above 0.3 T. This possibility was also suggested by the fact that the scaled data of $\phi_\sigma$ at $B=1$ T were more scattered than those at $B=0$ T, leading to poorer fitting results of $\omega_0$ and $\sigma_0$ to the 3D-*XY* model. As one possible candidate, we suspect that the vortex dynamics dominates the data. Indeed, the estimated $\xi(T)\sim 100$ nm for the 2D-"U" critical charge dynamics at 1.02 $T_c$ exceeds $\ell_v\sim 80$ nm at 0.3 T. However, we found that the scaled data of $\phi_\sigma$ for $x=0.17$ above 0.3 T were qualitatively different from those observed for $x=0.07$ at 1 T, as shown in Figs. 11 and 18. In addition, if we use the 3D-*XY* critical exponent, $\xi(T)$ in the measurement temperature range is estimated at most $\sim 60$ nm, which is smaller than $\ell_v\sim 80$ nm at 0.3 T. Therefore, there is another possibility that the critical charge dynamics changed from the 2D-"U" to the 3D-*XY* universality class, even though it remains unclear at present why the critical charge dynamics for $x=0.17$ was largely dependent on the applied magnetic field.

In summary, the systematic studies of the effects of the external magnetic field on the critical charge dynamics confirmed that our determination of the universality class, which was classified into 2D-*XY* for the underdoped region, 3D-*XY* for the optimally doped region, and 2D-"U" for the overdoped region, was plausible.

## V. DISCUSSION

As was already pointed out, we discovered three different universality classes in the phase diagram of LSCO, representing the existence of two kinds of crossover lines across the phase diagram. One is the dimensional crossover from 2D-*XY* to 3D-*XY* between $x=0.14$ and $x=0.15$, while the other is the crossover from 3D-*XY* to 2D-"U" between $x=0.16$ and $x=0.18$. The study of the effects of thickness and magnetic field dependence supported that these features were not caused by the finite-size effects, but were intrinsic to the superconducting phase transition in LSCO. In this section, we discuss possible origins of these changes of the universality class with the Sr concentration from various points of views.

### A. 2D-*XY* critical charge dynamics in the underdoped region

First, we discuss the 2D-*XY* critical charge dynamics in the underdoped region ($x=0.07-0.14$). This possibility was already pointed out by our previous study.[20] In this work, we confirmed that the exponential divergence of $\xi_{KT}(T)$ for $x=0.07$ was suppressed by applying small magnetic field, in agreement with the BKT theory which considered the effects of externally induced vortices.[47] These results strongly support that the critical charge dynamics in the underdoped region was classified into the 2D-*XY* universality class. What is most significant is that the phase fluctuations of the superconductivity order parameter, which could be directly determined in our methods,[48] survived only up to much lower temperature (at most $\sim 1.4$ $T_c$) than the closing temperature of the pseudogap. As shown in Fig 7, this shows a sharp contrast to the Nernst experiments by Ong and Wang.[49] Our results indicated that the anomalous pseudogap phenomena cannot be explained only by the classical phase fluctuations of superconducting orders, in contrast to the early prediction by Emery and Kivelson.[3] A similar conclusion was also obtained by a theoretical consideration on "cheap" vortices where the vortex core energy is very small ($\sim k_BT_c$) and both of the amplitude and phase fluctuations are controlled by the same energy scale, $k_BT_c$.[50]

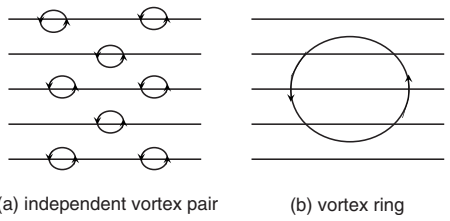


FIG. 20. Schematic drawings of (a) independent vortex-antivortex pair and (b) vortex ring in a layered superconductor.

In the layered superconductor, it is suggested that the finite interlayer coupling effect enhances the true critical temperature, $T_c$, as follows:

$$T_c/T_{BKT} = 1 + \left(\frac{\pi}{\ln\sqrt{1/\Delta}}\right)^2, \tag{11}$$

where $T_{BKT}$ and $\Delta$ are the BKT transition temperature and the anisotropy ratio of the interlayer coupling to the intralayer coupling, respectively.[51,52] According to Eq. (11), the 2D-*XY* critical behavior is no longer observed in the vicinity of $T_c$ and that the system should exhibit the 3D critical behavior, except for the case that the interlayer coupling is negligibly small ($\Delta\sim 0$). However, it should be pointed out that Eq. (11) overestimated $T_c$. In fact, Eq. (11) was derived by considering the critical radius, $r_c$, where the energy of the independent vortex pair balances with that of the vortex ring (see Fig. 20). In Refs. 51 and 52, $r_c$ was estimated by neglecting the contribution of the vortex core energy, $E_c$, compared to the logarithmic interaction term. However, this is incorrect, which was already pointed out in the original paper of the BKT theory[21] and also in a recent theoretical review paper more clearly.[50] Particularly, according to the latter paper, $E_c$ is expected to be at least comparable to the logarithmic interaction term even for cheap vortices. Thus, it is clear that Eq. (11) overestimates the enhancement of $T_c$ owing to the interlayer coupling effect. In order to discuss

the possibility of the vortex ring excitation in the layered cuprate superconductor more precisely, we need the accurate estimation of $E_c$ of cheap vortices, which remains an open issue.

Even if we consider a somewhat unrealistic situation where $E_c$ is negligible, our results merely suggest that the interlayer Josephson coupling is not yet developed at least above the minimum temperature where the critical behavior was successfully observed $\sim 1.01T_c$ for $x=0.07$, as shown in Fig. 7. Indeed, we found that the effective thickness of the superconducting sheet was comparable to the distance between the $CuO_2$ planes, suggesting that the fluctuating superconductivity appeared in each $CuO_2$ plane which remained nearly decoupled within the measured temperature range.[20] We emphasize that our results do not rule out the development of the interlayer Josephson coupling, which will finally lead to the 3D critical behavior. The Josephson coupling is expected to be developed in the further vicinity of $T_c$, which we could not approach experimentally. Thus, our observation of the 2D critical behavior does not contradict the general property of a layered superconductor.

### B. Two crossovers in the phase diagram

The most important findings are the two crossovers, that is, the crossover from 2D-*XY* to 3D-*XY* near $x=0.14$ (Ref. 20) and the other crossover from 3D-*XY* to 2D-"U" near $x=0.16$ in the phase diagram. First, we focus on the first crossover. The sudden change of the universality class from the 2D-*XY* to 3D-*XY* around at $x=0.14$ is discussed in terms of several theoretical models.

In the $U(1)$ mean-field theory of the $t-J$ model,[1,2] $T_c$ is controlled by the Bose condensation of holon in the underdoped region and the fermion pairing in the overdoped region. This means that a qualitative change of the condensation nature is expected to take place at the optimal doping. Our results were consistent with this picture in the sense that the critical charge dynamics changes near the optimally doped region. However, it seems to be difficult to explain the change of the dimensionality. In the theory, the weak 3D interlayer hopping is assumed to obtain a finite transition temperature of the Bose condensation of holons. As was suggested by Lee and co-workers,[50] the BKT transition for the fermion pairing and the boson condensation can occur simultaneously where the gauge field becomes massive due to the Higgs mechanism. Thus, the phase-transition lines for the fermion pairing and the boson condensation, which were predicted in the $U(1)$ mean filed theory of the $t-J$ model, become the crossover lines and only the superconducting transition remains to be the real BKT transition. This suggests that we should observe only the 2D-*XY* universality class in the whole range of the phase diagram. In other words, the anomalous change of the dimensionality in the critical behavior with carrier doping cannot be explained only by the early framework in the $t-J$ model suggesting the fermion pairing and the boson condensation. The so-called confinement-deconfinement transition due to the strong-coupling gauge field[50,53] is another candidate for the change of the critical behavior. Although a confinement-deconfinement transition does not always imply the change of the dimensionality, it is possible that a 3D Fermi-liquid phase is realized as a consequence of the confinement of fermions and bosons, in which the 3D-*XY* critical behavior arises.

On the other hand, in the hidden QCP scenario, this sudden change of the universality class can be understood as a classical-quantum crossover which may occur with $x$ approaching the hidden QCP located beneath the superconducting dome. A spatial and time correlation of the quantum fluctuation of the hidden order is strong near the QCP. Therefore, provided that the quantum fluctuation couples to the thermal fluctuation of the superconducting order, the critical dynamics around the superconducting transition can be affected by the quantum-fluctuation effects in the vicinity of the QCP. In this picture, it is also predicted that the quantum-fluctuation effects should become less prominent as $x$ increases away from the hidden QCP. From this point of view, the behavior in the overdoped region reported in this paper is very crucial to examine these theoretical models.

In the overdoped region, we found the second crossover from 3D-*XY* to 2D-"U" near $x=0.16$, in addition to the first crossover near $x=0.14$. This is highly unexpected, since the general trend is that the transport properties of the high-$T_c$ cuprates become less anisotropic with carrier doping.[54] The $t-J$ model based interpretation encounters a difficulty since it does not expect any further dimensional crossover to take place. Even if a 3D Fermi-liquid phase was realized by a confinement of fermions and bosons, there is no reason why the 3D phase is realized only in a narrow range near the optimally doped region. On the other hand, the theoretical models assuming the hidden QCP can naturally explain our finding that the critical charge dynamics at least down to $T \sim 1.01\ T_c$ was essentially 2D all over the phase diagram except for a narrow range near the optimally doped region. This result was in correspondence with the expectation that the quantum-fluctuation effects are prominent only in the vicinity of the QCP.

More precisely, the quantum-fluctuation effects at finite temperatures are prominent only in the *quantum critical region*, which will be described below. In general, in the 2D-QPT scenario, the hidden order of the QPT becomes long range only at zero temperature.[18] For instance, suppose the Heisenberg antiferromagnet with the 2D square lattice, which corresponds to an undoped $CuO_2$ plane.[55] The magnetic long-range order is present only for $g<g_c$ at $T=0$, where $g$ and $g_c$ are a key parameter to control a QPT and a critical parameter corresponding to the QCP, respectively. At $T=0$, the correlation length $\xi_Q$ of QPT diverges as $\sim|g-g_c|^{-\tilde{\nu}}$ in the vicinity of $g_c$, where $\tilde{\nu}$ is a static quantum critical exponent. On the other hand, at finite temperatures, there are three characteristic regions, each of which is separated by two crossover lines, $T=\pm(g-g_c)^{\tilde{\nu}\tilde{z}}$, where $\tilde{z}$ is a dynamic quantum critical exponent, as shown in Fig. 21. Here, we used the same description for each region as that proposed by Sachdev,[18] since the commonly used description such as "quantum disordered" seemed to be somewhat misleading.

In the *low* $T$ region on the magnetically ordered side $[0<T<(g_c-g)^{\tilde{\nu}\tilde{z}}]$, both of $\xi_Q$ and the correlation time, $\tau_Q$, de-

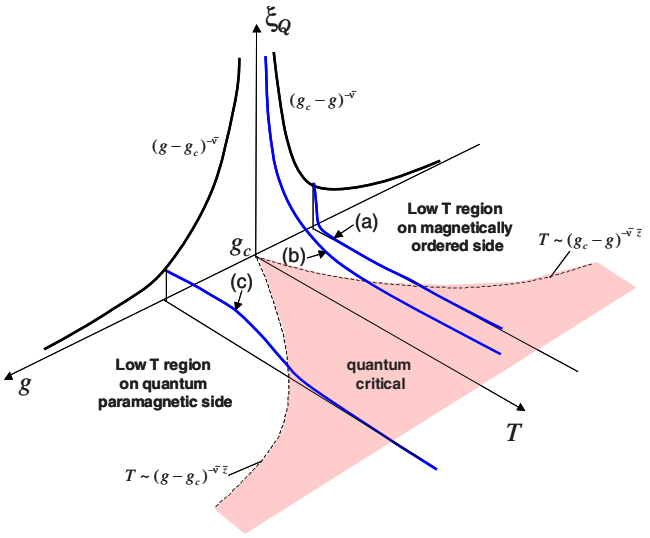


FIG. 21. (Color online) Schematic phase diagram of the 2D quantum antiferromagnet. Lines (a)–(c) represent $\xi_Q$ in each region.

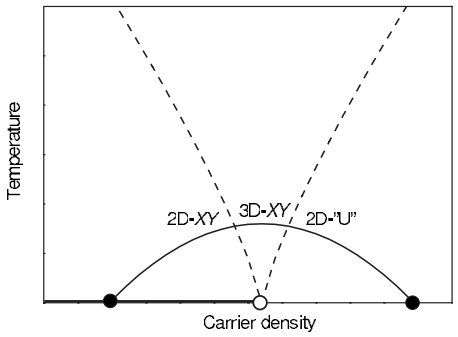


FIG. 22. Schematic phase diagram of LSCO together with our results about the critical charge dynamics. Solid circles are the phenomenologically well-established QCPs. An open circle near the optimal doping is a hidden QCP assumed to explain our findings. The region between two dashed lines is the *quantum critical region*. Thick solid line at $T=0$ is a long range ordered region.

crease exponentially as $T$ increases, suggesting that the quantum-fluctuation effect is extremely small [line (a) in Fig. 21]. Thus, in this region, the system is regarded as classical at finite temperatures. In the *quantum critical region* [$T>(g_c-g)^{\bar{\nu}\bar{z}}$ and $T>(g-g_c)^{\bar{\nu}\bar{z}}$], $\xi_Q$ and $\tau_Q$ decrease as $\sim 1/T$ [line (b) in Fig. 21]. This means that large quantum fluctuations survive even at high temperature which might appear in various properties, as well as thermal fluctuations. Finally, in the *low T* region on the quantum paramagnetic side [$0<T<(g-g_c)^{\bar{\nu}\bar{z}}$], $\xi_Q$ exponentially reaches a constant value as $T\rightarrow 0$ [line (c) in Fig. 21]. The value of $\xi_Q$ at $T=0$ behaves as $|g-g_c|^{\bar{\nu}\bar{z}}$. This region can also be regarded as a "spin liquid" state,[50] since there is no long-range order even at $T=0$. In this region, although quantum fluctuations surviving at $T=0$ contribute to the oscillatory spin correlation, the long-range time correlation is exponentially relaxed by thermal fluctuations. Thus, the behavior of $\tau_Q$ at $T>0$ is rather dominated by the classical relaxation. In summary, the schematic behavior of $\xi_Q$ for the 2D Heisenberg antiferromagnet is shown in Fig. 21.

When this concept is applied to discuss the phase diagram of the cuprates, the parameter, $g$, is related to the carrier concentration, $n$. As holes are doped into the $CuO_2$ plane at $T=0$, it is expected that the long-range order of the spin correlation is broken at a critical value of the hole doping, $n_c$, which is corresponding to $g_c$. Thus, one can consider that $g$ is a positive function of the hole doping and that $g(n_c)=g_c$. In the quantum critical region around $n_c$, the antiferromagnetic quantum fluctuation is considered to decay slowly as $\sim 1/T$. It is already well established that the antiferromagnetic quantum fluctuation favors the $d$-wave superconductivity.[4,5] This suggests the possibility that a spatial and time correlation of the superconducting order can be enhanced by the quantum-fluctuation effects. Provided that the interlayer correlation is also enhanced, the observed dimensional crossover from 2D to 3D can be understood as a consequence of these quantum-fluctuation effects. Note that this effect is limited to the quantum critical region. In other two regions, $\tau_Q$ for the quantum fluctuation decays exponentially with increasing temperature, suggesting a purely classical dynamics. Thus, the experimental result that the 3D behavior was observed only in the vicinity of the optimally doped region showed good qualitative agreement with this QCP scenario, as shown in Fig. 22.

Note that the 2D antiferromagnetic order discussed here is just one of the candidates for the possible QPT. The scenario is essentially based on a hidden order in the 2D system. The 2D order is present only at $T=0$ and becomes short range at finite temperatures, independent of $g$. Therefore, no experiment at finite temperatures can determine $n_c$ directly. This means that the disappearance of the 3D Néel order by hole doping does not always imply the position of the QCP in the 2D antiferromagnet. Rather, a scaling analysis of the wave vector- and frequency-dependent magnetic fluctuations seems to be useful to search the position of the QCP. Indeed, the neutron-scattering study using an LSCO single crystal suggested that the QCP might be hidden near $x=0.14$,[12] which agrees well with our results.

At present, this scenario seems to be compatible with our results most successfully. The important requirement is that the quantum fluctuation around the hidden QCP couples to the thermal fluctuations of the superconducting order near the superconducting transition. Thus, a crucial question is what is the most plausible candidate for a hidden order among various proposals.[4–11] A very recent discovery,[56] of the $4a_0$ wide unidirectional electronic domain which was detected by using a tunneling-asymmetry imaging technique in STM, may be also a candidate for such hidden orders. Unfortunately, we could not find a clear answer to this question in this work. In addition, there is a more complicated problem in the neighborhood of the Mott insulator-to-metal transition. It is predicted that the coupling between the order parameter of the QPT and the low-energy fermions provides a more complex behavior with two dynamic quantum critical exponents.[57–59] In LSCO single crystals, the insulator-to-metal crossover was suggested to occur near $x=0.16$ by the in-plane resistivity measurements down to $T=0.65$ K using a 61 T pulse magnetic field.[60] An open issue is whether this behavior is attributed to the Mott transition or not.

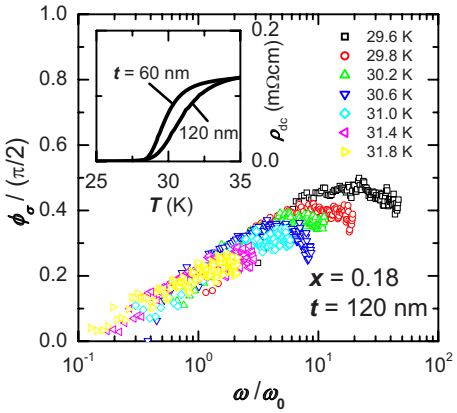


FIG. 23. (Color online) An example of the breakdown of the dynamic scaling for the $\phi_\sigma$ of the thicker film ($t$=120 nm) with $x$ =0.18. Inset: Temperature dependence of dc resistivity of the film compared to that of the thinner film ($t$=60 nm).

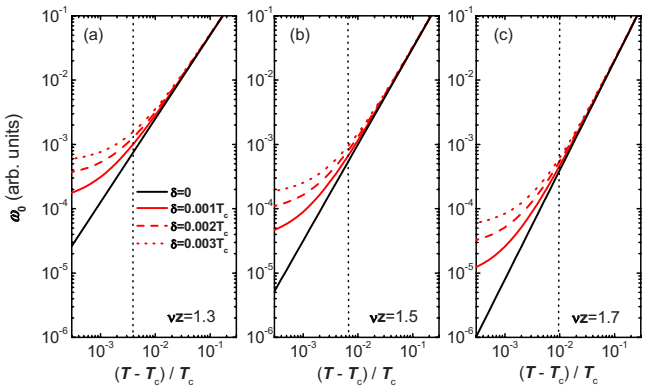


FIG. 24. (Color online) Temperature dependence of $\omega_0$ with $\xi$ diverging at $T_c-\delta$ for several values of $\nu z$ and $\delta$, where $\delta$ represents the width of the smeared $T_c$. A vertical dotted line in each panel represents a temperature, $T_L$, above which the power-law behavior of $\omega_0$ was observed in the zero magnetic field measurement for $x$ =0.18.

### C. Possible origin on the 2D-"U" critical charge dynamics

The critical charge dynamics observed in the overdoped region was found to be different from the well-known universality classes (2D-*XY*, 3D-*XY*, or the Gaussian fluctuation). Here, we discuss this 2D-"U" critical behavior in details.

First of all, we consider the effect of disorder due to the Sr substitution, which is expected to be more prominent with increasing Sr concentration. As was emphasized repeatedly, the successfully scaled data confirmed that the observed 2D-"U" critical behavior could not be explained by the distribution of $T_c$ due to the disorder effect because our method to obtain the data collapse of $\phi_\sigma$ and $|\sigma|$ is sensitive to the breakdown of the dynamic scaling hypothesis, which can be caused by a broad distribution of $T_c$ due to disorders. Figure 23 shows an example of the breakdown of the dynamic scaling due to the distribution of $T_c$. This is $\phi_\sigma(\omega)$ scaled by $\omega_0$ of the thicker film ($t$=120 nm) with $x$=0.18. As shown in the inset of Fig. 23, dc resistivity showed a broader transition width than that of the thinner film ($t$=60 nm), which yielded the successfully scaled $\sigma_{\rm fl}(\omega)$. It is clear that the data collapse of $\phi_\sigma(\omega)$ for the thicker film becomes worse with decreasing temperature, suggesting that a broad distribution of $T_c$ due to disorder results in the breakdown of the dynamic scaling hypothesis.

The plots of Fig. 7 are also suggestive to consider the influence caused by the distribution of $T_c$. Although a lower bound of the hatched region in Fig. 7 seems to show our experimental limitation to approach the critical region as close as possible, it may be explained by another possibility that it is determined by the influence of the slight distribution of $T_c$. In such a case, we can estimate the distribution of $T_c$ as follows. If a lower bound of the smeared $T_c$ was given by $T_c-\delta$, the critical behavior of $\omega_0$ or $\sigma_0$ with $\xi$ diverging at $T_c-\delta$ deviates from a power-law behavior below a temperature in the vicinity of $T_c$. For instance, in the case of $x$ =0.18, the power-law behavior with $\nu z=1.5\pm0.2$ down to $T_L=(1.007\pm0.003)T_c$ at $B$=0 T, where the error bars of $\nu z$ and $T_L$ were derived from the ambiguity of $T_c^{\rm scale}$. This suggests that the deviation from the power-law behavior due to the distribution of $T_c$ should be observed below $T_L$. Figure 24 shows the calculation of $\omega_0$ with $\xi$ diverging at $T_c-\delta$ for several values of $\nu z$ and $\delta$, indicating that the deviation occurs at a higher temperature with increasing the values of $\nu z$ and $\delta$. Thus, we found that $\delta$ for $x$=0.18 was less than 0.001 $T_c$(<0.03 K) even for the maximum value of $\nu z$, suggesting that the distribution of $T_c$ was negligibly small even for the overdoped LSCO.

In addition to such an experimental justification, the so-called Harris's criterion on the critical phenomenon also tells us that the weak disorder is irrelevant to the 2D-*XY* or 3D-*XY* critical behavior.[61] On the other hand, the strong disorder can change the critical behavior to a different one. However, even for the strong disorder, it seems difficult to change the dimensionality in the critical charge dynamics. In other words, the observed dimensional crossover from 3D to 2D is a very robust one, which cannot be explained by the disorder effect.

Meanwhile, the strong disorder effect is one of the possible candidates for the origin of the anomalous critical exponents. The disorder effect on the 2D system has been investigated by the 2D random gauge *XY* model, which introduced the disorder effect as the random variables in magnetic bond angles uniformly distributed in the range from $-r\pi$ to $r\pi$.[62] When the disorder strength, $r$, is equal to 1, the model corresponds to the standard *XY* gauge glass model,[63] while the standard *XY* model is recovered for $r$=0. Interestingly, a recent Monte Carlo simulation of the 2D random gauge *XY* model suggested that a non-BKT type transition with $\nu\approx1.1$ occurred at low temperatures for a stronger disorder strength than a critical value of $r$, while the standard BKT transition occurred at low temperatures for a weaker disorder strength.[62] The calculated critical exponent is not so different from our result ($\nu\sim0.9$) for $x$=0.18. Thus, this is one possibility for the 2D-"U" universality class. However, a better agreement of the critical exponent is obtained by considering the frustration effect on the 2D system. We will discuss this later in terms of the frustrated 2D-*XY* model.

Next, in the $t-J$ model assuming the BKT transition for the fermion pairing and the boson condensation, it is ex-

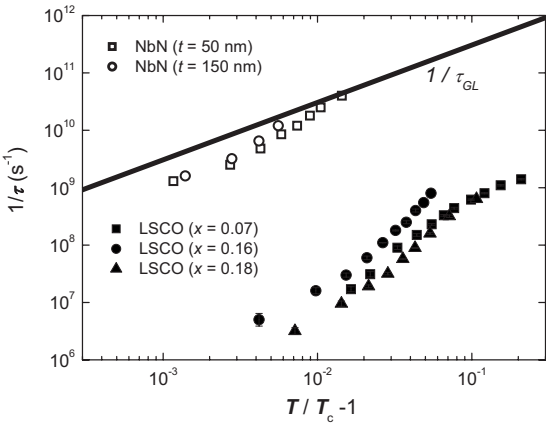


FIG. 25. Temperature dependence of $1/\tau$, where $\tau$ is the correlation time. Solid symbols are data of LSCO films ($x=0.07,0.16,0.18$) in this work and open symbols are data of NbN films ($t=50$ nm, 150 nm) in Ref. 24. Error bars were estimated through those for $\omega_0$, which were estimated by using the methods described in the Appendix. A solid straight line is $1/\tau_{\mathrm{GL}}$ given by Eq. (12).

pected that the 2D-*XY* critical behavior is observed in a whole region of the phase diagram. In practice, the BKT transition cannot be observed unless the BKT criterion, $\lambda_\perp \gg L$, is satisfied,[21] where $\lambda_\perp (=\lambda^2/D_s)$ and $L$ are a screening length and a lateral size of a superconducting sheet, respectively, and $\lambda$ and $D_s$ are a bulk penetration depth and a thickness of the superconducting sheet, respectively. In the underdoped region, this criterion is satisfied, indeed.[20] For overdoped films, $\lambda_\perp$ was estimated to be $10\sim100$ mm, which is sufficiently larger than $L\sim1$ mm, showing the criterion is satisfied also for overdoped samples. Therefore, the 2D-"U" critical behavior was not induced by the failure of the BKT criterion. Thus, the 2D-"U" feature cannot be explained by the $t-J$ model based theories.

In a model assuming that a Fermi-liquid state is realized in the heavily overdoped region, one may expect that a conventional Gaussian fluctuation rather than the critical fluctuation becomes more prominent with increasing the Sr concentration. From this point of view, a crossover from the 2D-*XY* critical behavior to the Gaussian fluctuation can be a candidate for the origin of the observed anomalous critical exponents. In order to examine this, we estimated $1/\tau$ for each film ($\tau$ is the correlation time of the fluctuation) by comparing the scaled data of $\phi_\sigma(\omega)$ to the Gaussian scaling function.[43] In the GL theory assuming the Gaussian fluctuation, it is well known that the divergence of $\tau$ near $T_c$ is given as follows:

$$\tau_{\mathrm{GL}} = \frac{\pi\hbar}{16k_B|T-T_c|}. \tag{12}$$

Surprisingly, we found that all the results of $1/\tau$ for $x=0.07$, 0.16, and 0.18 were much smaller than $1/\tau_{\mathrm{GL}}$ by 2 or 3 orders of magnitude, as shown in Fig. 25. A similar slow critical charge dynamics has been reported for the nearly optimally doped $YBa_2Cu_3O_y$ thin film.[23] These results show a sharp contrast to the similar plots of $1/\tau$ for NbN thin films,[24] which almost agreed with $1/\tau_{\mathrm{GL}}$ (also shown in Fig. 25). Therefore, the observed dynamics is indeed attributed to the *critically slowing down* phenomenon in the critical region and it cannot be explained by a crossover to the Gaussian fluctuation. Interestingly, such a slow dynamics is also expected in the low $T$ regions both on the magnetically ordered and the quantum paramagnetic sides around the QCP because of the opening of an energy gap in the excitation spectrum.[18]

In terms of the QCP scenario, we believe that the spin liquid state in the low $T$ region on the quantum paramagnetic side seems to provide key information to understand the origin of the 2D-"U" critical behavior. When a hole is doped in the $CuO_2$ plane, the spin on a Cu site is combined to the spin of the doped hole to form the Zhang-Rice (ZR) singlet,[64] giving rise to the spatial modulation of the nearest-neighbor exchange interaction, $J$, to a square lattice in the $CuO_2$ plane. In other words, the formation of the ZR singlet by doped holes introduces the frustration between the spins in the 2D antiferromagnet, as pointed out by Anderson.[65] In particular, mobile ZR singlets can give rise to the dynamic spin frustration. This dynamic or static frustration effect has been considered to play an essential role in stabilizing the spin liquid or glass state.[65,66] Such a frustrated state might be related to the 2D-"U" critical behavior in the overdoped region. Thus, we need to consider more explicitly the influence of the frustration effect to the superconductivity realized in the quantum paramagnetic side.

The static frustration effect in the *XY* spin systems has been extensively investigated by the so-called frustrated *XY* model[67] both theoretically[68] and experimentally.[69] Interestingly, the study of the critical behavior in frustrated *XY* spins seems to suggest the possibility of a new universality class, which is clearly different from the 2D-*XY* universality class.[68] Indeed, many numerical simulations for the fully frustrated *XY* model suggested that $\nu=0.8-1.0$,[68] which shows a good agreement with our result ($\nu\sim0.9$) for $x=0.18$. Although the explicit correspondence between the frustrated *XY* spin system and the superconductivity realized in the spin liquid state is an open issue to be resolved, the resemblance between the critical behaviors of both systems suggests the importance of frustration effect in the overdoped region.

## VI. CONCLUSION

We investigated the critical charge dynamics of the superconducting to the normal-state transition for LSCO thin films with a wide range of the Sr concentration ($x=0.07-0.20$) through the dynamic scaling analysis of the fluctuation-induced microwave conductivity. We discovered that the critical charge dynamics in the phase diagram of LSCO was classified into the following three different universality classes: (i) the 2D-*XY* universality class for the underdoped region ($x=0.07-0.14$), (ii) the 3D-*XY* universality class for the nearly optimally doped region ($x=0.15$ and 0.16), and (iii) the 2D-"U" ($\nu=0.9\pm0.05$, $z=1.7\pm0.3$) universality class for the overdoped region ($x=0.17-0.20$). We confirmed that the anomalous 2D critical behavior for the overdoped

region is not induced by the finite-size effect but is intrinsic to the overdoped LSCO.

Our results indicated that there are two kinds of dimensional crossovers in the phase diagram of LSCO, suggesting that the dimensionality in the critical charge dynamics changes twice with hole doping. In other words, except for the 3D-*XY* critical charge dynamics observed only near the optimally doped concentration, we found that the critical charge dynamics of LSCO was essentially two dimensional. This suggests that the fluctuating high-temperature superconductivity initially appears in each $CuO_2$ plane, preceding the development of the interlayer Josephson coupling. Our results for the underdoped LSCO also indicated that the 2D-*XY* critical charge dynamics could be observed at most up to $\sim 1.4T_c$, which was much lower than a closing temperature of the pseudogap. Thus, some of the early naive pictures about the pseudogap and the critical fluctuations in high-$T_c$ cuprates need to be modified.

We discussed the possible origins of the anomalous dimensional crossovers. It is concluded that neither the weakened anisotropic property with hole doping nor the confinement-deconfinement transition discussed in the $t-J$ model can explain the second dimensional crossover from the 3D-*XY* to the 2D-"U", which occurs between $x=0.16$ and 0.17. On the other hand, the so-called hidden QCP scenario, where the quantum critical fluctuation near the hidden QCP couples to the superconducting fluctuation, was able to explain the existence of two kinds of dimensional crossovers qualitatively. This scenario also seems to provide a key information to understand the origin of the 2D-"U" critical behavior, whose critical exponents were found to be similar to those of the frustrated *XY* model. The importance of the frustration effect in the spin liquid state is implied

At present, the scenario based on a hidden order of QPT in the 2D system seems to be the most reasonable candidate for the anomalous change of the universality class with hole doping. However, the hidden order which provides the direct evidence for QCP has not been yet discovered. If the hidden order is formed in the 2D system, it will be almost impossible to be found at finite temperatures. Thus, the dynamic scaling analysis including the quantum critical fluctuations plays an important role to settle this issue.

## ACKNOWLEDGMENTS

We thank H. Fukuyama, Y. Matsuda, and K. Fukushima for fruitful discussions and comments. This work was partly supported by the Grant-in-Aid for Scientific Research (Grants No. 13750005, No. 15760003, No. 17038006, No. 17340102, and No. 19014005) from the Ministry of Education, Science, Sports and Culture of Japan. T.O. thanks the Japan Society for the Promotion of Science for financial support.

## APPENDIX

In the present study, the scaling procedures described in Sec. II were usually performed by eyes. However, the noises appeared in the scaled data of $\phi_\sigma$ and $|\sigma|$ often make a reliable estimation of errors on scaling parameters quite difficult. In this appendix, we describe another methods to perform the scaling procedure, which enable to estimate the error bars on the scaling parameters, $\omega_0$ and $\sigma_0$. If the most appropriate scaling function is already known, the least-squares minimization of the residuals is very useful. However, this means that one must assume a plausible scaling function before performing the scaling procedure. This is not a completely independent analysis we propose, but the same as the conventional analysis assuming the dimensionality or the critical exponents. As an alternative method without assuming any scaling function, we propose the following two methods to check the data collapses and to evaluate their error bars.

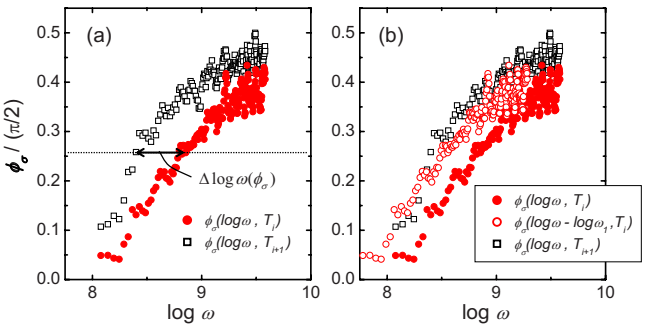


FIG. 26. (Color online) (a) The first method (method I) and (b) the second method (method II) to check data collapses and to evaluate their error bars.

The first method (method I) is performed as follows. After the frequency dependence of $\phi_\sigma(\omega)$ at each temperature is converted to the data sets of $\log \omega(\phi_\sigma)$ as a function of $\phi_\sigma$, the difference of $\log \omega(\phi_\sigma)$ showing the same $\phi_\sigma$ between the adjacent temperatures is calculated, as shown in Fig. 26(a). When we describe it as $\Delta \log \omega(\phi_\sigma)$, the mean value of $\Delta \log \omega(\phi_\sigma)$ gives the difference of $\log \omega_0$ between the adjacent temperatures, where $\omega_0$ is the scaling parameter. Thus, the error bars of $\log \omega_0$ are given by the standard deviation of $\Delta \log \omega(\phi_\sigma)$. The other scaling parameter, $\log \sigma_0$, and its error bars can also be estimated by repeating similar procedures for the data sets of $|\sigma(\omega/\omega_0)|$.

This method was found to provide almost the same results as those obtained from the scaling procedures by eyes when the presence of noise was less prominent. In our measurement technique, the noises that appeared in $\phi_\sigma$ and $|\sigma|$ are mainly attributed to the slight ripple structure remained after the calibration. Thus, we made the averaging or smoothing procedure on the data of $\phi_\sigma(\omega)$ and $|\sigma(\omega)|$ before performing the scaling procedures by method I.

Although the averaging or smoothing procedure is useful to suppress noises, such secondary data treatments may break the intrinsic properties included in the original data. The second method (method II) was developed to avoid the averaging or smoothing procedure in the scaling of $\phi_\sigma$, as described below. First, we plot the data of $\phi_\sigma$ as a function of $\log \omega$, as shown in Fig. 26(b). Next, the $i$th data of $\phi_\sigma(\log \omega)$ at a temperature $(T=T_i)$ are shifted along the $\omega$ direction by a test value, $\log \omega_1$. We describe it as $\phi_\sigma(\log \omega_i - \log \omega_1, T_i)$. Finally, a square of the difference between

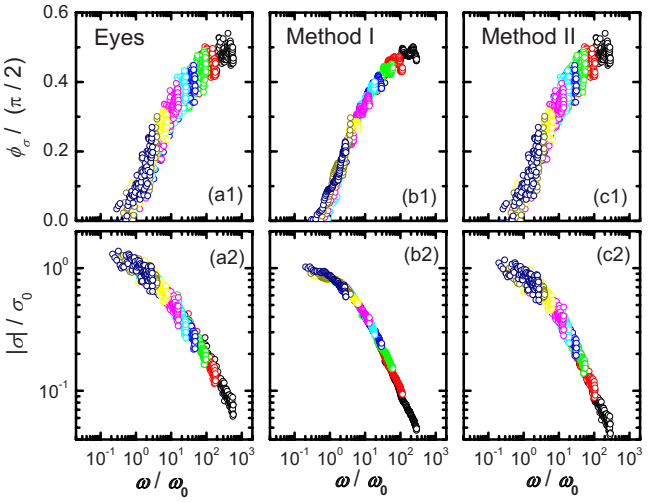


FIG. 27. (Color online) Comparison among three methods of the scaling procedures which were performed on the data of $\phi_\sigma$ (upper panels) and $|\sigma|$ (lower panels) for $x=0.16$ in zero magnetic field. Here, the plots of scaled data were obtained by eyes (a1 and a2), by method I (b1 and b2), and method II (c1 and c2), respectively.

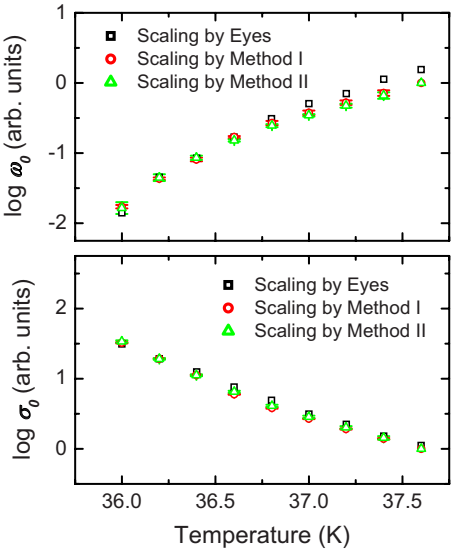


FIG. 28. (Color online) Temperature dependence of the scaling parameters of $\omega_0$ (upper panel) and $\sigma_0$ (lower panel), which were obtained for $x=0.16$ in zero magnetic field.

$\phi_\sigma(\log \omega_i - \log \omega_1, T_i)$ and $\phi_\sigma(\log \omega_i)$ at the adjacent temperature $(T=T_{i+1})$ is summed up in the frequency range where the data sets of $\phi_\sigma(\log \omega)$ at both temperatures are overlapped. When we describe it as $Y(\omega_1)(\equiv\Sigma_i[\phi_\sigma(\log \omega_i - \log \omega_1, T_i) - \phi_\sigma(\log \omega_i, T_{i+1})]^2)$, the scaling parameter, $\omega_0$, is determined by the definition that $\omega_0$ is equal to the test value giving the minimum of $Y(\omega_1)$. In practice, the second-ordered least-squares minimization technique was used to determine the minimum of $Y(\omega_1)$ more precisely. Thus, we used the difference between $\omega_0$ and the test value of $\omega_1$, which gave the minimum among the discrete sets of $Y(\omega_1)$, as a measure of the error bars on $\omega_0$.

Figures 27 and 28 show the comparison among three methods of the scaling procedures, which were performed for $x=0.16$ in zero magnetic field. We confirmed that not only the data collapse of $\phi_\sigma$ and $|\sigma|$ but also the temperature dependence of $\omega_0$ and $\sigma_0$, which were obtained by both methods (method I and method II), showed a good agreement with those obtained from the scaling procedures by eyes. Similar results were obtained for other samples. Therefore, it is clear that our conclusions are not changed by the methods to perform the scaling procedures.

*hkitano@phys.aoyama.ac.jp

[1] Y. Suzumura, Y. Hasegawa, and H. Fukuyama, J. Phys. Soc. Jpn. **57**, 2768 (1988).
[2] N. Nagaosa and P. A. Lee, Phys. Rev. Lett. **64**, 2450 (1990); P. A. Lee and N. Nagaosa, Phys. Rev. B **46**, 5621 (1992).
[3] V. J. Emery and S. A. Kivelson, Nature (London) **374**, 434 (1995).
[4] T. Moriya, Y. Takahashi, and K. Ueda, J. Phys. Soc. Jpn. **59**, 2905 (1990).
[5] P. Monthoux, A. V. Balatsky, and D. Pines, Phys. Rev. Lett. **67**, 3448 (1991).
[6] C. Castellani, C. DiCastro, and M. Grilli, Phys. Rev. Lett. **75**, 4650 (1995).
[7] C. M. Varma, Phys. Rev. B **55**, 14554 (1997).
[8] S. Chakravarty, R. B. Laughlin, D. K. Morr, and C. Nayak, Phys. Rev. B **63**, 094503 (2001).
[9] J. Zaanen, Nature (London) **404**, 714 (2000).
[10] S. A. Kivelson, E. Fradkin, V. Oganesyan, I. P. Bindloss, J. M. Tranquada, A. Kapitulnik, and C. Howald, Rev. Mod. Phys. **75**, 1201 (2003).
[11] M. Vojta, Y. Zhang, and S. Sachdev, Phys. Rev. Lett. **85**, 4940 (2000).
[12] G. Aeppli, T. E. Mason, S. M. Hayden, H. A. Mook, and J. Kulda, Science **278**, 1432 (1997).
[13] T. Valla, A. V. Fedorov, P. D. Johnson, B. O. Wells, S. L. Hulbert, Q. Li, G. D. Gu, and N. Koshizuka, Science **285**, 2110 (1999).
[14] J. L. Tallon, J. W. Loram, G. V. M. Williams, J. R. Cooper, I. R. Fisher, J. D. Johnson, M. P. Staines, and C. Bernhard, Phys. Status Solidi **215**, 531 (1999) .
[15] F. F. Balakirev, J. B. Betts, A. Migliori, S. Ono, Y. Ando, and G. S. Boebinger, Nature (London) **424**, 912 (2003).
[16] D. van der Marel, H. J. A. Molegraaf, J. Zaanen, Z. Nussinov, F. Carbone, A. Damascelli, H. Eisaki, M. Greven, P. H. Kes, and M. Li, Nature (London) **425**, 271 (2003).
[17] Y. Ando, S. Ono, X. F. Sun, J. Takeya, F. F. Balakirev, J. B. Betts, and G. S. Boebinger, Phys. Rev. Lett. **92**, 247004 (2004).
[18] S. Sachdev, *Quantum Phase Transition* (Cambridge University Press, Cambridge, England, 1999).
[19] D. S. Fisher, M. P. A. Fisher, and D. A. Huse, Phys. Rev. B **43**, 130 (1991).
[20] H. Kitano, T. Ohashi, A. Maeda, and I. Tsukada, Phys. Rev. B

**73**, 092504 (2006).
[21] V. L. Berezinskii, Sov. Phys. JETP **32**, 493 (1970); J. M. Kosterlitz and D. J. Thouless, J. Phys. C **6**, 1181 (1973).
[22] P. M. Chakin and T. C. Lubensky, *Principles of Condensed Matter Physics* (Cambridge University Press, Cambridge, England, 1995).
[23] J. C. Booth, D. H. Wu, S. B. Qadri, E. F. Skelton, M. S. Osofsky, A. Piqué, and S. M. Anlage, Phys. Rev. Lett. **77**, 4438 (1996).
[24] T. Ohashi, H. Kitano, A. Maeda, H. Akaike, and A. Fujimaki, Phys. Rev. B **73**, 174522 (2006).
[25] For example, D. R. Strachan, M. C. Sullivan, P. Fournier, S. P. Pai, T. Venkatesan, and C. J. Lobb, Phys. Rev. Lett. **87**, 067007 (2001); D. R. Strachan, C. J. Lobb, and R. S. Newrock, Phys. Rev. B **67**, 174517 (2003), and references therein.
[26] For a review, Q. Li, in *Physical Properties of High Temperature Superconductors V*, edited by D. M. Ginsberg (World Scientific, Singapore, 1996), p. 209.
[27] For example, A. Junod, M. Roulin, B. Revaz, and A. Erb, Physica B **280**, 214 (2000); M. V. Ramallo and F. Vidal, Phys. Rev. B **59**, 4475 (1999), and references therein.
[28] V. Pasler, P. Schweiss, C. Meingast, B. Obst, H. Wühl, A. I. Rykov, and S. Tajima, Phys. Rev. Lett. **81**, 1094 (1998); C. Meingast, V. Pasler, P. Nagel, A. Rykov, S. Tajima, and P. Olsson, *ibid.* **86**, 1606 (2001).
[29] For example, S. Kamal, D. A. Bonn, N. Goldenfeld, P. J. Hirschfeld, R. Liang, and W. N. Hardy, Phys. Rev. Lett. **73**, 1845 (1994); S. M. Anlage, J. Mao, J. C. Booth, D. H. Wu, and J. L. Peng, Phys. Rev. B **53**, 2792 (1996); J. R. Waldram, D. M. Broun, D. C. Morgan, R. Ormeno, and A. Porch, *ibid.* **59**, 1528 (1999); K. M. Paget, B. R. Boyce, and T. R. Lemberger, *ibid.* **59**, 6545 (1999).
[30] P. C. Hohenberg and B. I. Halperin, Rev. Mod. Phys. **49**, 435 (1977).
[31] I. Tsukada and S. Ono, Phys. Rev. B **74**, 134508 (2006).
[32] I. Tsukada, Phys. Rev. B **70**, 174520 (2004).
[33] A. N. Lavrov, I. Tsukada, and Y. Ando, Phys. Rev. B **68**, 094506 (2003).
[34] S. Komiya, Y. Ando, X. F. Sun, and A. N. Lavrov, Phys. Rev. B **65**, 214535 (2002); J. Takeya, Y. Ando, S. Komiya, and X. F. Sun, Phys. Rev. Lett. **88**, 077001 (2002).
[35] H. Sato and M. Naito, Physica C **274**, 221 (1997); H. Sato, A. Tsukada, M. Naito, and A. Matsuda, Phys. Rev. B **61**, 12447 (2000).
[36] I. Bozovic, G. Logvenov, I. Belca, B. Narimbetov, and I. Sveklo, Phys. Rev. Lett. **89**, 107001 (2002).
[37] Y. Ando, S. Komiya, K. Segawa, S. Ono, and Y. Kurita, Phys. Rev. Lett. **93**, 267001 (2004).
[38] H. Kitano, T. Ohashi, H. Ryuzaki, A. Maeda, and I. Tsukada, Physica C **412-414**, 130 (2004).
[39] J. C. Booth, D. H. Wu, and S. M. Anlage, Rev. Sci. Instrum. **65**, 2082 (1994).
[40] H. Kitano, T. Ohashi, and A. Maeda, Rev. Sci. Instrum. **79**, 074701 (2008).
[41] D. M. Pozar, *Microwave Engineering* (Wiley, New York, 1998).
[42] M. L. Stutzman, M. Lee, and R. F. Bradley, Rev. Sci. Instrum. **71**, 4596 (2000).
[43] H. Schmidt, Z. Phys. **216**, 336 (1968).
[44] The preliminary results for $x=0.19$ were already published. See also T. Ohashi, H. Kitano, A. Maeda, and I. Tsukada, Physica C **460-462**, 906 (2007).
[45] R. A. Wickham and A. T. Dorsey, Phys. Rev. B **61**, 6945 (2000).
[46] W. L. Johnson, C. C. Tsuei, and P. Chaudhari, Phys. Rev. B **17**, 2884 (1978).
[47] S. Doniach and B. A. Huberman, Phys. Rev. Lett. **42**, 1169 (1979).
[48] H. Kitano, T. Ohashi, A. Maeda, and I. Tsukada, Physica C **460-462**, 904 (2007).
[49] N. P. Ong and Y. Wang, Physica C **408-410**, 11 (2004), and references therein.
[50] P. A. Lee, N. Nagaosa, and X. G. Wen, Rev. Mod. Phys. **78**, 17 (2006).
[51] S. Hikami and T. Tsuneto, Prog. Theor. Phys. **63**, 387 (1980).
[52] Y. Matsuda, S. Komiyama, T. Onogi, T. Terashima, K. Shimura, and Y. Bando, Phys. Rev. B **48**, 10498 (1993).
[53] N. Nagaosa and P. A. Lee, Phys. Rev. B **61**, 9166 (2000).
[54] For a review, S. L. Cooper and K. E. Gray, in *Physical Properties of High Temperature Superconductors IV*, edited by D. M. Ginsberg (World Scientific, Singapore, 1994), p. 61.
[55] S. Chakravarty, B. I. Halperin, and D. R. Nelson, Phys. Rev. B **39**, 2344 (1989).
[56] Y. Kohsaka, C. Taylor, K. Fujita, A. Schmidt, C. Lupien, T. Hanaguri, M. Azuma, M. Takano, H. Eisaki, H. Takagi, S. Uchida, and J. C. Davis, Science **315**, 1380 (2007).
[57] M. Vojta, Rep. Prog. Phys. **66**, 2069 (2003).
[58] A. Rosch, Phys. Rev. B **64**, 174407 (2001).
[59] M. Imada, Phys. Rev. B **72**, 075113 (2005).
[60] G. S. Boebinger, Y. Ando, A. Passner, T. Kimura, M. Okuya, J. Shimoyama, K. Kishio, K. Tamasaku, N. Ichikawa, and S. Uchida, Phys. Rev. Lett. **77**, 5417 (1996).
[61] A. B. Harris, J. Phys. C **7**, 1671 (1974).
[62] P. Holme, B. J. Kim, and P. Minnhagen, Phys. Rev. B **67**, 104510 (2003).
[63] D. A. Huse and H. S. Seung, Phys. Rev. B **42**, 1059 (1990).
[64] F. C. Zhang and T. M. Rice, Phys. Rev. B **37**, 3759 (1988).
[65] P. W. Anderson, Science **235**, 1196 (1987).
[66] S. F. Edwards and P. W. Anderson, J. Phys. F: Met. Phys. **5**, 965 (1975).
[67] J. Villain, J. Phys. C **10**, 1717 (1977); **10**, 4798 (1977).
[68] For example, M. Hasenbusch, A. Pelissetto, and E. Vicari, J. Stat. Mech.: Theory Exp. (2005) P12002, and references therein.
[69] For example, B. J. van Wees, H. S. J. van der Zant, and J. E. Mooij, Phys. Rev. B **35**, 7291 (1987); X. S. Ling, H. J. Lezec, M. J. Higgins, J. S. Tsai, J. Fujita, H. Numata, Y. Nakamura, Y. Ochiai, C. Tang, P. M. Chaikin, and S. Bhattacharya, Phys. Rev. Lett. **76**, 2989 (1996); J. Affolter, M. Tesei, H. Pastoriza, C. Leemann, and P. Martinoli, Physica C **369**, 313 (2002); H. Sano, A. Endo, S. Katsumoto, and Y. Iye, J. Phys. Soc. Jpn. **76**, 094707 (2007), and references therein.